energies

MDPI

Article

Optimal Scheduling of Regional Combined Heat and Power System Based on Improved MFO Algorithm

Fan Wang [1], Xiang Liao [1,*], Na Fang [1] and Zhiqiang Jiang [2]

[1] Hubei Engineering Research Center for Safety Monitoring of New Energy and Power Grid Equipment, School of Electrical & Electronic Engineering, Hubei University of Technology, Wuhan 430068, China; 102010336@hbut.edu.cn (F.W.); fangna@hbut.edu.cn (N.F.)

[2] School of Civil & Hydraulic Engineering, Huazhong University of Science & Technology, Wuhan 430068, China; zqjzq@hust.edu.cn

* Correspondence: liaoxiang@hbut.edu.cn; Tel.: +86-027-8801-3889

Abstract: Due to the inflexibility of cogeneration power plants and the uncertainty of wind power production, the excess power of the distribution network brings challenges to the power grid operation. This paper introduced an improved moth-flame optimization algorithm to meet the challenge of energy complementary dispatching. The proposed algorithm adopts three effective strategies, namely inertia weight, unified initialization, and the spiral position update strategy, which maintains a strong global search ability and a potent compromise between global and local search. The effectiveness of the proposed method was evaluated by benchmark functions. Furthermore, the proposed method was applied to combine heat and power system operation problems and economic dispatch in light load and wind power unpredictability. In order to verify the robustness of the algorithm and solve the complex constraints of power systems under extreme conditions, three different cases had been discussed. The experimental findings indicate that the proposed algorithm shows better performances in terms of convergence speed, ability to escape from a local optimum solution, and population diversity maintenance under different complexity conditions of engineering problems.

Keywords: combined heat and power plant; moth-flame optimization; intelligent optimization algorithm; inertial weight; integrated energy system

Citation: Wang, F.; Liao, X.; Fang, N.; Jiang, Z. Optimal Scheduling of Regional Combined Heat and Power System Based on Improved MFO Algorithm. *Energies* **2022**, *15*, 3410. https://doi.org/10.3390/en15093410

Academic Editors: Dimitrios Katsaprakakis and Massimo Dentice D'Accadia

Received: 21 March 2022
Accepted: 26 April 2022
Published: 6 May 2022

1. Introduction

Because of the rising cost of energy and the limited availability of fossil-fuel energy, systems that are more efficient, such as cogeneration, have become more popular. At present, the energy utilization rate of most power plants is less than 60%, but the fuel utilization rate of cogeneration units is as high as 90%, and it can reduce 13–18% of the pollutants (CO_2, SO_2, SO_x and NO_x). With the increasingly serious environmental problems, reducing the use of fossil fuels and improving fuel utilization has become a consensus. However, when the cogeneration units with nonlinear and non-convex characteristics exist, making the best possible use of the electrical system is becoming more and more difficult. It is a nonlinear, multi-constraint, and non-convex optimization problem to solve the economic dispatch optimization issue of combined heat and power (CHPED). The key is to minimize the total cost and meet the power and heat demand of the system considering the constraints of the unit [1]. With the traditional pure mathematical optimization algorithm, it is difficult to solve this problem. Many researchers have proposed different optimization methods by applying heuristic algorithms. Motevasel et al. [2] used the Modified Bacterial Foraging Optimization Algorithm. Then, there are the ant colony optimization algorithm and simulated annealing algorithm [3], the Non-dominated Sorting Genetic Algorithms-II [4], multi-objective particle swarm optimization [5], distributed proximal strategy optimization [6], genetic algorithm [7], and so on.

In northern China, coal, oil, and wind energy resources are abundant, while other resources are relatively scarce. Power generating equipment is mainly composed of large thermal power units. However, due to the influence of winter temperature, the demand for heat load is large, so most of the installed units have the function of cogeneration, which effectively improves the energy utilization rate. In reality, the operation condition of cogeneration units is greatly constrained by the heat load, and the heat load is only borne by the heat output of cogeneration, which directly leads to the decrease of peak regulation capacity of units, resulting in large wind curtailment loss. Therefore, reasonable optimal scheduling of cogeneration units and wind turbines has an important impact on improving power system efficiency. Many scholars have researched this field. Iterative methods are used to solve the CHPED model presented by Li et al. [8]. The model considers the temperature dynamics of the district heating system and uses energy storage as a choice to solve the optimization problem for managing wind energy variability. Luo et al. [9] established a two-way conversion system for cogeneration by charging gas, fuel elements, and heat preservation devices in the cogeneration organization to realize the two-way conversion of electricity and gas and the decoupling of the two operation modes of cogeneration units, which greatly improved the adaptability of the system to extra wind power. Niknam, Azizipanah-Abarghooee, Roosta and Amiri [1] considered the uncertainty of wind power output, combined with the operation price model of wind and thermal power, constructed the multi-objective dynamic optimization scheduling model considering unit commitment, and used the multi-objective particle swarm optimization algorithm through priority ranking and multi-subgroup co-evolution to solve the model. There are also some references introducing electric boilers and heat storage systems in the arrangement to effectively enhance the degree of adaptability of the system of combined heat and power (CHP) units and reduce wind abandonment [10,11].

The main topic of this paper is the moth-flame optimization algorithm. Mirjalili [12] presented a novel metaheuristics optimization algorithm based on the navigation strategy of moths in nature. One of its most appealing features is that it requires no derivation of information in the starting phase. In addition, it has a small number of parameters, and is easy to implement, scalable, and flexible. So far, a variety of methods for solving optimization issues, including binary, real (continuous), constraint, single-objective, multi-objective, and multimodal moth-flame algorithm (MFO), have been developed. Several research articles have been discussed and summarized. However, the algorithm also has some defects and shortcomings.

The algorithm's convergence speed has little effect on its performance. To accelerate the algorithm's convergence and allow moths to find the optimal solution faster, many researchers have carried out a lot of research. Shehab et al. [13] applied the local-based algorithm to MFO and added six popular solution selection schemes. The results show that the proportional selection scheme has a fast search speed and high quality of solution selection. Abd Elaziz et al. [14] mixed opposition-based learning technology and differential evolution technique with MFO to increase the algorithm's quick convergence. The experimental results show that this algorithm is superior to the existing meta-heuristic algorithm in the performance index and optimal subset. Wu et al. [15] designed the moth moves straight to the optimal position, and then added Levy flights to enhance the moth-flame optimization technique. The identification results are compared to other optimization approaches to validate the improved algorithm's efficacy.

The original moth-flame optimization algorithm's convergence rate is too quick throughout the running process, and it is prone to enter a local optimum, resulting in the inability to provide a high-quality optimal solution. Numerous research works have been conducted to address this issue. Pelusi et al. [16] defined the mixed stage between exploration and development by updating the fitness weight factor of moth position. The results show that the post-well algorithm has achieved the best results in terms of searchability and convergence performance. Nguyen et al. [17] mixed the Lévy flight and the logarithmic function to improve the convergence rate of the algorithm by using its flame

update formula. The comparison results show that the improved algorithm achieves better results than other algorithms in the competition. Taher et al. [18] improved the effectiveness and robustness of the algorithm by changing the path of the moth forming a new spiral around the flame. Dabba et al. [19] introduced a population-intelligent gene selection algorithm based on the hybrid of quantum computing and moth flame optimization algorithm—quantum moth flame optimization algorithm (QMFOA). QMFOA was tested on 13 microarray datasets. The results showed that QMFOA had higher classification accuracy and the ability to reduce the number of selected genes compared with other algorithms.

Another problem of MFO is the lack of exploration ability. The flight range of moths is not large enough, and the searchability is indirectly affected. There are still some defects in the ability and range of finding solutions. Li et al. [20] introduced two new effective strategies, Levy Flights and Dimension-by-Dimension Evaluation, to maintain a strong global search capability and an effective balance between global search and local search. Kaur et al. [21] increased the Cauchy distribution function to improve the exploration ability and the best flame effect to improve the exploration efficiency, and uses the adaptive step size and iterative division to maintain the balance between exploration and exploitation. Pradhan et al. [22] proposed the orthogonal moth flame optimization algorithm and added the concept of orthogonality. Statistical measures, convergence analysis, and complexity measures show that the algorithm can effectively solve practical optimization problems.

The aforementioned methods tend to enhance the exploration ability of the algorithm. However, sometimes the consideration of diversity is insufficient. For instance, Sheng et al. [23] proposed a double flame generation strategy to generate two different types of target flame to guide the moth's flight. In addition, two different renewal strategies are proposed to update the location of moths to maximize the balance between development and exploration. The results show that the algorithm proposed in this paper has better diversity and performance compared to other mature methods. Xu et al. [24] adopted the Gaussian variation method to improve the population diversity of MFO. Then, a chaotic local search is applied to the MFO flame update process to better excavate the locality of the solution. Yu et al. [25] proposed an improved moth flame optimization algorithm based on an annealing strategy and quantum rotation gate, which improved the advantages of the algorithm in the local development process. The two engineering problems of feature selection, pressure vessel design, and multi-disc clutch braking are effectively solved.

The main work of this paper is to improve the newly proposed moth-fire optimization algorithm and to study the application of this algorithm in the related optimization problems of multi-energy scheduling complementarity in power systems. The research work is mainly reflected in the following aspects: the mathematical model of the optimization mechanism of the improved moth-flame optimization algorithm and the research into the optimization performance of the algorithm. This paper also proposes the research on multi-energy complementary scheduling engineering of power system based on improved mothball optimization algorithm in extreme environment.

2. Moth-Flame Optimization

The MFO algorithm [12] sees moths as a potential solution and their position in space as the variable. The moth may therefore exist in multiple dimensions by altering its location vector. Because the MFO approach uses swarm intelligence, the population of moths may be expressed as Equation (1) in the matrix. The description of related symbols is given in Table A1.

$$M = \begin{bmatrix} m_{1,1} & m_{1,2} & \cdots & m_{1,d} \\ m_{2,1} & m_{2,2} & \cdots & m_{2,d} \\ \vdots & \vdots & \vdots & \vdots \\ m_{n,1} & m_{n,2} & \cdots & m_{n,d} \end{bmatrix} \quad (1)$$

Among them, n is the number of moths, whereas d denotes the number of control variables in the dimension of the optimization problem. Additionally, a column of fitness value vectors corresponding to these moths is predicted, as indicated in Equation (2).

$$OM = \begin{bmatrix} OM_1 \\ OM_2 \\ \vdots \\ OM_n \end{bmatrix} \tag{2}$$

To avoid entering a local optimum and significantly increase the individual's universal search capabilities, the MFO approach mandates that each moth updates its position using just the matching unique flame. As a consequence, the flame position and the moth location in the search space are both variable vectors of the same dimension, which are expressed as Equation (3).

$$\mathrm{F} = \begin{bmatrix} F_{1,1} & F_{1,2} & \cdots & F_{1,d} \\ F_{2,1} & F_{2,2} & \cdots & F_{2,d} \\ \vdots & \vdots & \vdots & \vdots \\ F_{n,1} & F_{n,2} & \cdots & F_{n,d} \end{bmatrix} \tag{3}$$

Additionally, it is hypothesized that these flames correlate to a column in the fitness vector, which is expressed as Equation (4).

$$OF = \begin{bmatrix} OF_1 \\ OF_2 \\ \vdots \\ OF_n \end{bmatrix} \tag{4}$$

Variables in the two matrices have distinct updating strategies throughout the iteration. The flame represents the ideal location that has been repeatedly optimized so far, and the moth represents a seeking person traveling around the search space. A similar flame surrounds each moth. It is updated to the location of the flame in the following generation whenever a better solution has been identified. The algorithm will virtually never miss a chance to locate the global optimum solution in the optimization method if this approach is used. The location update method of each moth relative to the flame may be described by Equation (5) in order to develop a mathematical model of moth flying behavior in response to the flame

$$M_i = S(M_i, F_j) \tag{5}$$

where Mi denotes the ith moth, Fj represents the jth flame, and S stands for the spiral function. Equation (7) defines the spiral function of the moth's flight path. This is presented in Figure 1.

$$D_i = \left|F_j - M_i\right| \tag{6}$$

$$S\left(M_i, F_j\right) = D_i \times e^{bt} \times cos(2\pi t) + F_j \tag{7}$$

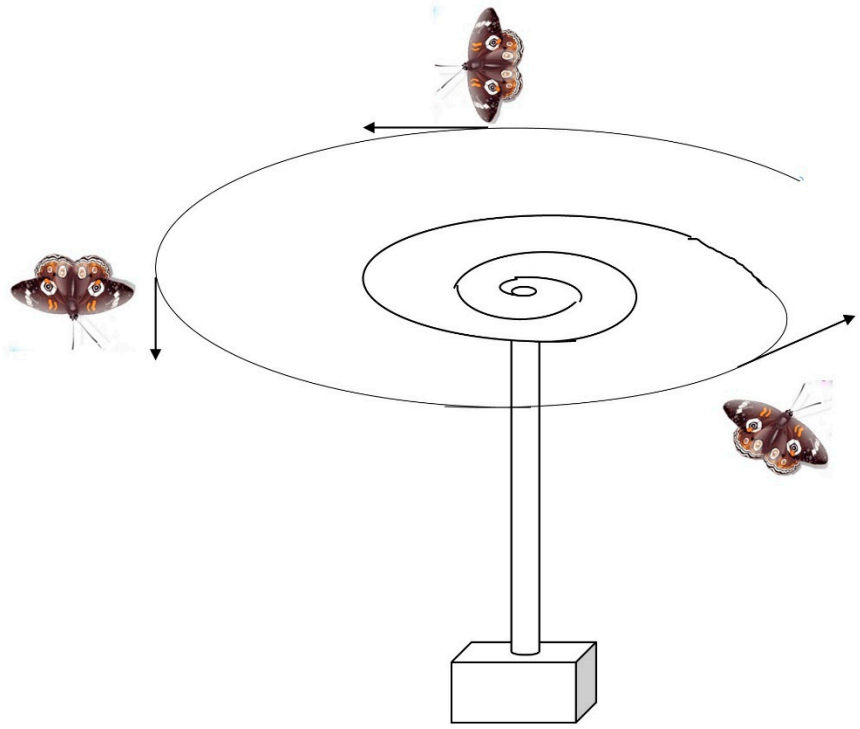

Figure 1. The flight trajectory of moths around the light source.

t donates a random number between $[-1, 1]$ in the interval between the ith moth and the jth flame, and Di specifies the linear distance between the ith moth and the jth flame.

3. The Proposed Methods

This section discusses the three critical components that comprise the MFO and explains how they work. Finally, the suggested method's computational complexity is evaluated.

3.1. Uniform Initialization

Random initialization, chaotic initialization, and opposition-based initialization do not effectively alleviate the problem of aggregation of moths in the process of finding solutions, which directly leads to moths in the local optimum for a long time so that they cannot reach the global optimum quickly and accurately. It is also possible that some regions are skipped to explore, while other regions conduct multiple searches, which greatly prolongs the search time of the moth and reduces its search efficiency. In this paper, the unified initialization method of the moth is adopted to make the moth more fully traverse the entire exploration area. The first row randomly selects the position of the moth X = [X11, X12, . . . , X1D] as the base point. To guarantee the unpredictability of the moth solution, Row 2–4 creates a D(n − 1) random matrix R = [R1, R2, . . . , RD]. Lines 5–12 divide each dimension's length by n to get the shortest distance between moths in that dimension. Moths are uniformly dispersed in each dimension in lines 5–12 to avoid moth aggregation into a local optimum [26].

3.2. Inertial Weights

The fundamental cause of the MFO algorithm's early convergence is usually thought to be a lack of population variety. As a result, its diversity is critical to the population optimization procedure. When a population has a lot of variety, it will try to expand its range in a small space. To put it another way, a high population diversity indicates that a big portion of the search space has been explored. The algorithm's search space shrinks due to the fast loss of variety in the evolution process. Moth location updates are grouped into

two kinds in MFO. Each moth flies around the appropriate flame and updates its location when the number of moths is less than or equal to the number of flames. When the number of moths exceeds the number of flames, the adaptive flame reduction method forces all moths to use the same flame update point. The inertia weight of real-time feedback control is introduced to the first scenario in this study, and the moth's update relation is Equation (8).

$$S(M_i, F_j) = \omega \times D_i \times e^{bt} \times \cos(2\pi t) + F_j \tag{8}$$

The lower the ω number, the more probable that all populations in the search space will converge to the ideal place. Equation (9) proposes an inertia weight.

$$\omega = \frac{e^{2(1-T/T\max)} - e^{-2(1-T/T\max)}}{e^{2(1-T/T\max)} + e^{-2(1-T/T\max)}} \tag{9}$$

3.3. Dynamic Variable Spiral Position Update Strategy

The moth will change the traveling distance of each position update throughout the seeking process based on the spiral shape between the flame location and its position. This is presented in Figure 2. Dynamic programming is used to tackle the issue of decision process optimization [27]. In the spiral pathfinding Equation (8), b is a constant that controls the spiral shape, which is generally set to a constant, and the speed of each position update is adjusted according to different spiral radians. However, setting b to a constant value will result in the moth's spiral movement being too singular during the search process, each time following the fixed spiral close to the target, making it easy to fall into the misunderstanding of the local optimal solution and weakening the algorithm's global search capability. To address this issue and allow the moth to build more different search pathways for position updating, we present the concept of variable spiral search [28]. This work enhanced the technique, optimized the moth's flying route, and significantly increased the moth's seeking efficiency. Argument b is intended to be a variable that varies in value as the number of iterations increases. The spiral form of the moth is constantly altered to maximize the moth's capacity to explore the unknown region, which consequently improves the algorithm's global search capability. Equation (10) is as follows after merging adaptive weights:

$$\begin{cases} S(M_i, F_j) = \omega \times D_i \times e^{bt} \times \cos(2\pi t) + F_j \\ b = e^{k \times \sin(\Pi \times (1 - (\frac{t}{t\max})))} \end{cases} \tag{10}$$

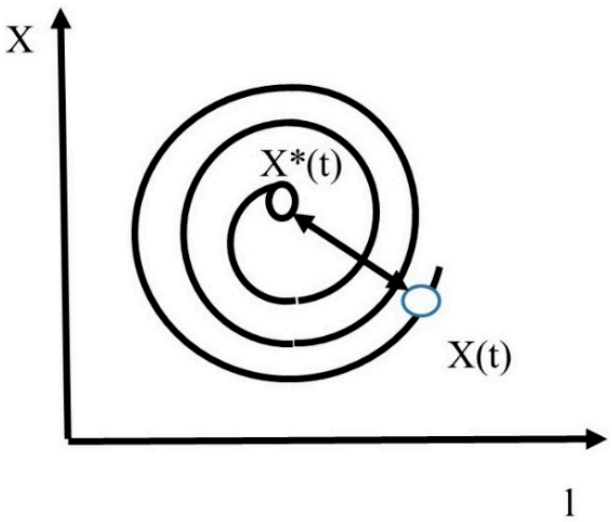

Figure 2. Position variation diagram.

b is modeled after the spiral mathematical model. The spiral form is dynamically modified based on the initial spiral model by adding the iterations. The factor *b* will grow in value as the number of generations increases, resulting in a spiral form that transitions from big to tiny. The moth hunts for the target with a huge spiral form early in the algorithm, and the moth explores the global optimum solution as much as possible to increase the algorithm's global optimal search capability. Later in the process, the moth explores the target with a little spiral form to increase the program's optimization accuracy.

This paper uses the above three mechanisms to propose an improved moth fire suppression algorithm (IUVMFO). To illustrate the mechanism of IUVMFO, the pseudocode of IUVMFO is shown below (Figure 3).

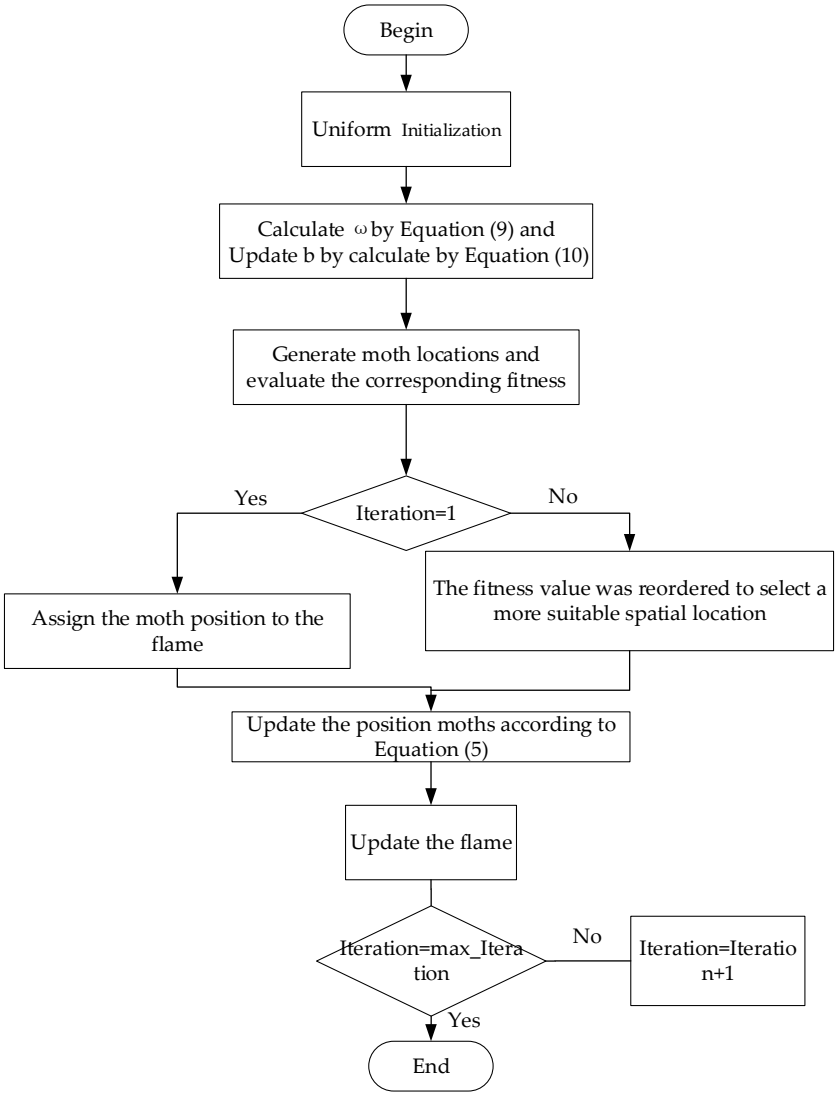

Figure 3. An enhanced moth-flame optimization algorithm (IUVMFO).

4. Case Study

4.1. Benchmark Function Test

This paper selects the benchmark function of CEC2017 to evaluate the suggested IUVMFO algorithm's performance and compares it with the standard MFO algorithm and moth-flame optimization algorithm based on diversity and mutation strategy (DMMFO) [29]. CEC2017 comprises four parts: three unimodal Functions (1–3), thirteen simple multimodal Functions (4–16), six hybrid Functions (17–21), and eight composite Functions (21–30). Detailed information on CEC2017 is introduced in Table A2.

4.1.1. Parameter Setting

The parameter setting of the metaheuristic algorithm affects the convergence performance. In Equation (9), the MFO algorithm's primary control parameter is b. The dynamic variable spiral strategy is used to adjust the path of the moth, and the dynamic factor k is used to adjust the parameter b. This parameter setting directly affects the shape of the number spiral curve. To investigate the effect of various k values on the algorithm and analyze the influence of the k value on the convergence of the algorithm, this article implements the enhanced algorithm for six distinct kinds of functions. Fixed parameters: n = 100, *MaxFEs* = 1000 dim. Tables 1–3 illustrate the test results for three distinct dimensions at various k values. When k = 5, the optimization results of five functions are the best. As the dimension increases, the convergence result of the F1 function is not ideal. However, F17 and F25 always show good test results, and the convergence results under other k values are not significantly different. So, the k value in this article is 5. To achieve fairer purposes, throughout this paper, all algorithms are performed in the same environment. Matlab2020b is used to execute all algorithms. Windows 10 is the operating system used in the simulation. The CPU is an Intel Core i7 running at 2.3 GHz. The experimental settings are as follows: population size equal to 50, *MaxFES* equal to 1000 dim. Each algorithm is independently executed 50 times and accumulates execution results on 10, 30, and 50 dimensions. Then, the collected results were statistically analyzed. All algorithms and their versions have control settings that are in line with the relevant research.

Table 1. The 10-dimensional function test.

Function		**10 dim**				
		k = 1	**k = 3**	**k = 5**	**k = 7**	**k = 9**
F1	Mean	5.521×10^3	5.468×10^3	5.583×10^3	3.750×10^3	6.906×10^3
	Std	5.058×10^3	5.402×10^3	4.366×10^3	4.420×10^3	5.301×10^3
F6	Mean	6.001×10^2	6.001×10^2	600	7.281×10^2	6.001×10^2
	Std	0.522	0.249	1.218×10^{-11}	1.234×10^{-6}	0.011
F17	Mean	1.741×10^3	1.739×10^3	1.737×10^3	1.739×10^3	1.739×10^3
	Std	20.683	15.619	10.212	13.445	17.566
F20	Mean	2.048×10^3	2.031×10^3	2.027×10^3	2.028×10^3	2.036×10^3
	Std	27.623	18.024	11.799	19.623	12.091
F25	Mean	2.917×10^3	2.938×10^3	2.942×10^3	2.899×10^3	2.937×10^3
	Std	24.231	20.089	13.389	23.692	19.885
F30	Mean	2.621×10^3	2.622×10^3	2.623×10^3	2.617×10^3	2.618×10^3
	Std	6.718	10.148	5.909	6.412	9.195

Table 2. The 30-dimensional function test.

Function		**30dim**				
		k = 1	**k = 3**	**k = 5**	**k = 7**	**k = 9**
F1	Mean	1.816×10^9	2.127×10^9	2.819×10^9	3.416×10^9	1.470×10^9
	Std	1.618×10^9	3.468×10^9	3.336×10^9	4.125×10^9	2.529×10^9
F6	Mean	6.147×10^2	6.162×10^2	6.121×10^2	6.124×10^2	6.125×10^2
	Std	7.670	14.072	7.161	5.631	8.181
F17	Mean	2.332×10^3	2.436×10^3	2.239×10^3	2.28×10^3	2.258×10^3
	Std	2.702×10^2	2.373×10^2	1.980×10^2	2.353×10^2	1.988×10^2
F20	Mean	2.587×10^3	2.564×10^3	2.547×10^3	2.550×10^3	2.679×10^3
	Std	2.350×10^2	1.803×10^2	1.780×10^2	2.317×10^2	2.718×10^2
F25	Mean	2.974×10^3	2.973×10^3	2.968×10^3	2.970×10^3	2.969×10^3
	Std	84.969	65.701	1.090×10^2	60.395	71.729
F30	Mean	2.783×10^3	2.775×10^3	2.772×10^3	2.773×10^3	2.782×10^3
	Std	25.436	24.722	27.266	34.693	22.763

Table 3. The 50-dimensional function test.

Function		50dim				
		k = 1	**k = 3**	**k = 5**	**k = 7**	**k = 9**
F1	Mean	1.670×10^{10}	1.092×10^{10}	1.517×10^{10}	1.156×10^{10}	1.267×10^{10}
	Std	1.076×10^{10}	5.565×10^{9}	8.465×10^{9}	4.889×10^{9}	6.986×10^{9}
F6	Mean	6.302×10^{2}	6.273×10^{2}	6.271×10^{2}	6.292×10^{2}	6.400×10^{2}
	Std	5.667	5.333	6.783	6.927	7.914
F17	Mean	3.606×10^{3}	3.487×10^{3}	3.485×10^{3}	3.830×10^{3}	3.580×10^{3}
	Std	3.899×10^{2}	3.773×10^{2}	3.743×10^{2}	3.911×10^{2}	4.064×10^{2}
F20	Mean	3.383×10^{3}	3.363×10^{3}	3.118×10^{3}	3.419×10^{3}	3.276×10^{3}
	Std	3.766×10^{2}	3.275×10^{2}	4.182×10^{2}	3.516×10^{2}	3.217×10^{2}
F25	Mean	4.331×10^{3}	4.019×10^{3}	3.603×10^{3}	3.664×10^{3}	3.645×10^{3}
	Std	1.161×10^{3}	8.093×10^{2}	3.735×10^{2}	3.921×10^{2}	3.872×10^{2}
F30	Mean	3.151×10^{3}	3.129×10^{3}	3.060×10^{3}	3.075×10^{3}	3.070×10^{3}
	Std	60.029	34.095	64.180	48.276	45.017

4.1.2. Evaluation Criteria

This article presents the generally used evaluation indices, such as the average convergence value and standard deviation, in order to assess the algorithm's performance. Both the standard deviation and the mean value indicate the accuracy of the algorithm in convergence tests. The Wilcoxon signed-rank test is also used in this work to compare the two methods in further detail. The algorithm's benefits and downsides are evaluated using a small sample size. Both algorithms' convergence results are paired and subtracted, and R+ and R are recorded as a consequence of this procedure for each test function. Generally speaking, when the number of R+ is more than the number of R, the former method is considered to be superior, and vice versa. The significance threshold is often set at 0.05 in this article. This work compares algorithms and uses symbols to show which ones are better ('+'), worse (i.e., '−'), and equal ('='). The entire difference between the symbols '+' and '−' is represented by gm.

4.2. The Problem of Economic Dispatch of Cogeneration

This problem was raised by Sohrabi et al. [30]. There are three units in this engineering problem, namely the pure power unit, CHP unit, and pure heat unit in Figure 4.

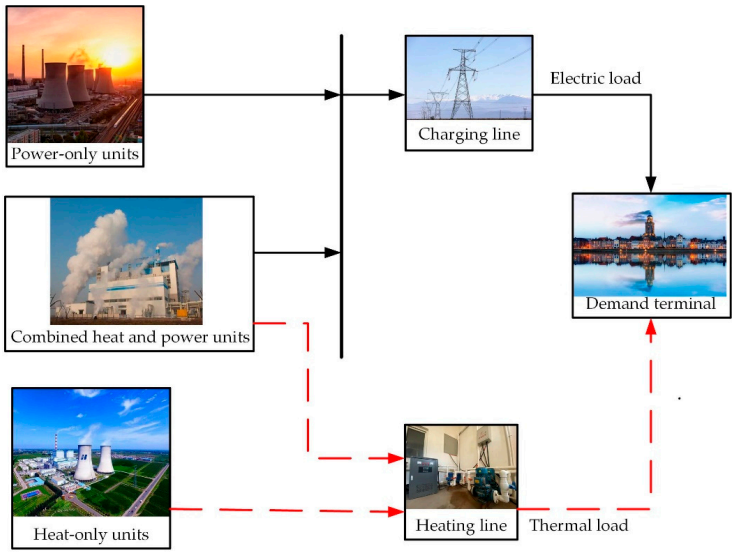

Figure 4. Cogeneration system.

The objective function of the problem is to minimize the operating cost of the system under constraint conditions. The objective function is defined as:

$$\mathrm{OF} = \sum_{m=1}^{N_p} C_m(P_m^p) + \sum_{n=1}^{N_C} C_n(P_n^c, H_n^c) + \sum_{n=1}^{N_h} C_s(H_s^h) \tag{11}$$

where $C_m(P_m^p)$ represents the cost of operation of the mth pure power unit generating P_m^p MW. $C_n(P_n^c, H_n^c)$ is defined as the operating cost of the nth cogeneration unit for the production of P_n^c MW power, and H_n^c MWth thermoelectric power. The operating cost of the pure heat unit in the production of H_s^h MWth thermal power is $C_s(H_s^h)$. N_p, N_c, and N_h are the total number of pure power, CHP, and pure heat units, m, n, and s are the indicators of the above units. The unit cost function is formulated as:

$$C_m(P_m^p) = \alpha_m(P_m^p)^2 + \beta_m P_m^p + \gamma_m \tag{12}$$

$$C_n(P_n^c, H_n^c) = a_n(P_n^c)^2 + b_n P_n^c + c_n + d_n(H_n^c)^2 + e_n H_n^c + f_n P_n^c H_n^c \tag{13}$$

$$C_s(H_s^h) = a_s(H_s^h)^2 + b_s H_s^h + c_s \tag{14}$$

In Equation (11), α_m, β_m, and γ_m are the calculation coefficients of the operation cost of the mth pure power unit. In Equation (12), a_n, b_n, c_n, d_n, e_n, and f_n are the constant cost coefficients related to the nth CHP unit, and a_s, b_s, and c_s are the operating cost function coefficients of sth pure heat units in Equation (13).

The total amount of electricity and heat generated by the system should fulfill the following power and heat requirements:

$$\sum_{m=1}^{N_P} P_m^p + \sum_{n=1}^{N_c} P_n^c = P_d + P_{loss} \tag{15}$$

$$\sum_{n=1}^{N_c} H_n^c + \sum_{s=1}^{N_h} H_s^h = H_d \tag{16}$$

P_d and H_d are the normal power demand and normal heat demand, respectively. P_{loss} is the transmission loss generated in the whole cogeneration. Power and heat generated by the power system should be within the acceptable range of each unit:

$$P_m^{p\min} \le P_m^p \le P_m^{p\max} \tag{17}$$

$$P_n^{c\min}(H_n^c) \le P_n^c \le P_n^{c\max}(H_n^c) \tag{18}$$

$$H_n^{c\min}(P_n^c) \le H_n^c \le H_n^{c\max}(P_n^c) \tag{19}$$

$$H_s^{h\min} \le H_s^h \le H_s^{h\max} \tag{20}$$

where $P_m^{p\min}$ and $P_m^{p\max}$ represent the lower limit and upper limit of pure power unit, respectively. $P_n^{c\min}$, $H_n^{c\min}$, and $H_n^{c\max}$ are the minimum and maximum electrical power and thermal power outputs of CHP units, respectively. In addition, $H_s^{h\min}$ and $H_s^{h\max}$ represent the lower and upper limits of pure thermal units, respectively.

A pure power unit, two cogeneration units, and a pure heat unit make up the whole cogeneration system. To simplify the computation process and to facilitate the calculation, this paper ignores the transmission loss of the power system. Demands for power and heat are 200 MW and 115 MW, respectively. Cost functions for pure power (Equation (21)) and pure thermal power (Equation (22)) units are considered linear.

$$C_1(P_1) = 50P_1; 0 \le P_1 \le 150 \tag{21}$$

$$C_4(H_4) = 23.4H_4; 0 \le H_4 \le 2695.2 \tag{22}$$

Cost coefficients of CHP units are shown in Table 4. In addition, the feasible thermoelectric operating area of CHP is shown in Figures 5 and 6.

Table 4. Cost coefficient of CHP unit.

Unit	*a*	*b*	*c*	*d*	*e*	*f*
2	0.0345	14.5	2650	0.03	4.2	0.031
3	0.0435	36	1250	0.027	0.6	0.011

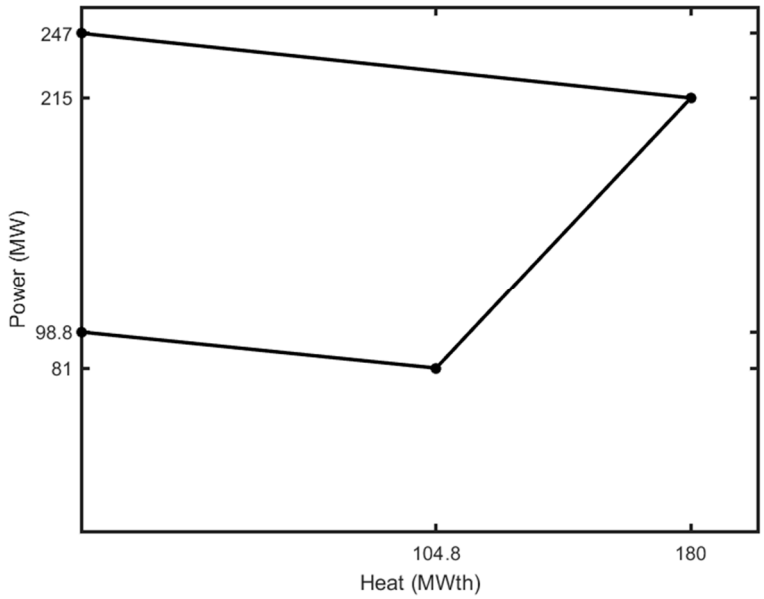

Figure 5. Feasible operating area of Heat-power in unit 2.

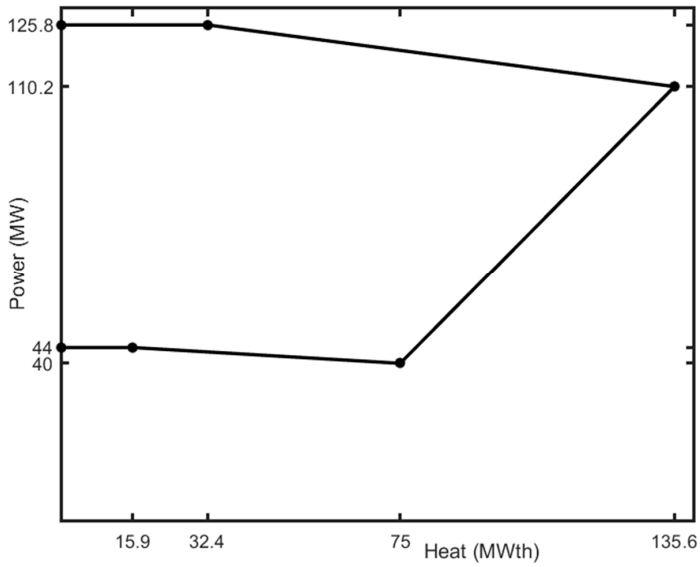

Figure 6. Feasible operating area of Heat-power in unit 3.

4.3. The Problem of Economic Dispatch in Light Load and Wind Power Unpredictability

This problem was raised by Pourghasem et al. [31]. The main objective of this engineering challenge is to find the best possible output from each unit for each hour and scenario, under the condition of meeting the requirements of electricity and heat load and other operational constraints. The whole system is composed of pure power, cogeneration, pure heat unit, and wind turbine in Figure 7.

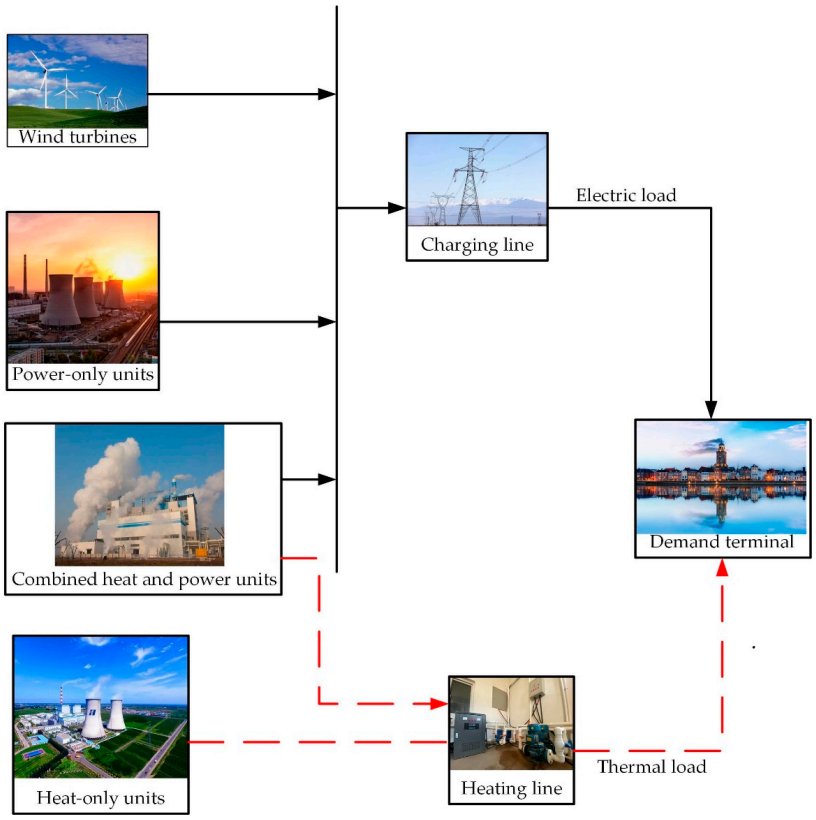

Figure 7. Energy dispatch system based on the unpredictability of load and wind power.

4.3.1. Scenario-Based Uncertainty Model

In this problem, power load demand and wind energy are uncertain. In order to model the uncertainty, this paper selects the scenario-based model and uses the wheel mechanism to generate the system demand scenario. Random variables with known probability density functions are used to represent the prediction error related to loading demand and wind power, and the probability density function of each random variable is discretized. The seven intervals in Figure 8 are centered on the zero means. The width of each interval is equal to the standard deviation (σ) of the prediction error, and σ is equal to 10% of the predicted value. The probability of each interval at time t is represented by $\alpha_{i,t}$. As shown in Equation (23), the sum of the cumulative probability of the interval is 1.

$$\sum_{i=1}^{7} \alpha_{i,t} = 1 \tag{23}$$

In order to create the scene required by the system, the random number in the interval [0, 1] is generated to compare with the cumulative probability starting from the last interval. Select the first interval where the cumulative probability is equal to or less than a random number, and the binary parameter associated with this interval becomes equal to 1. Therefore, as shown in Equation (24), each scene has a binary vector, which shows the binary parameters of power load demand and wind power interval.

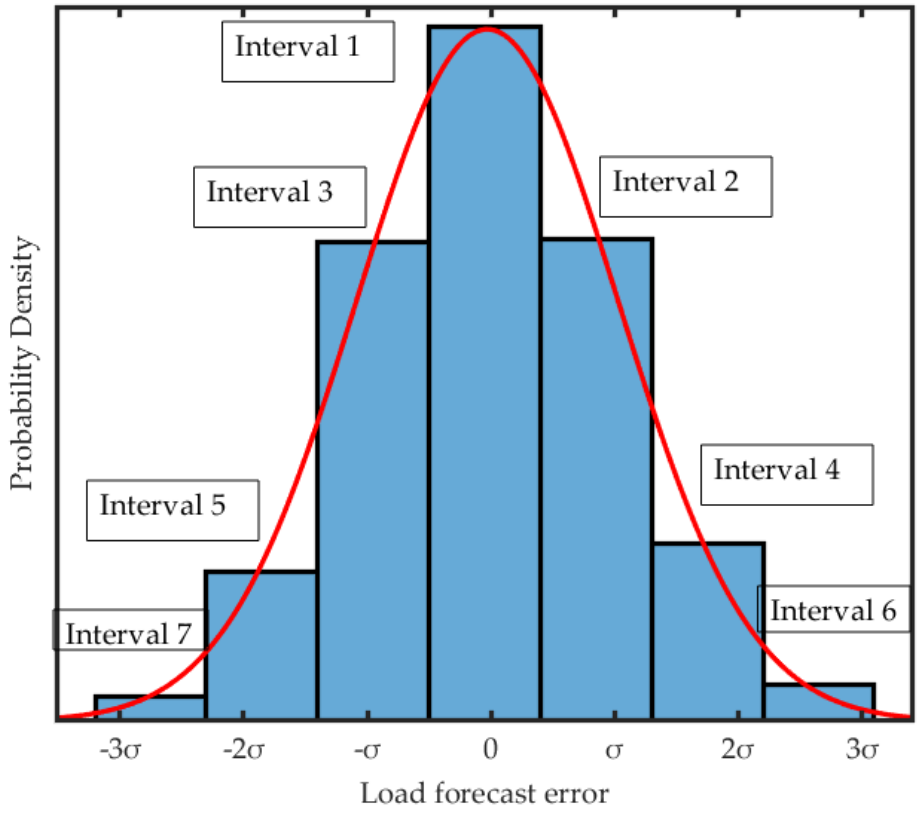

Figure 8. Discrete probability density function of load forecasting error.

$$scene(s) = \left[B^{L}_{(1,t,s)}, \cdots, B^{L}_{(7,t,s)}, \ldots, B^{W}_{(1,t,s)}, \cdots, B^{W}_{(7,t,s)}\right]_{t=1,\cdots,24} \tag{24}$$

$B^{L}_{(\text{interval},t,s)}$ and $B^{W}_{(\text{interval},t,s)}$ are binary parameters of power load demand and time t interval of wind power generation in scene s, respectively. The following formula calculates the probability of each scene

$$\pi_s = \frac{\prod_{t=1}^{24}\left(\sum_{m=1}^{7}\left(B^{L}_{\mathrm{m},t,s}\times\alpha_{\mathrm{m},t}\right)\times\sum_{n=1}^{7}\left(B^{W}_{n,t,s}\times\beta_{n,t}\right)\right)}{\sum_{s=1}^{N_s}\left(\prod_{t=1}^{24}\left(\sum_{m=1}^{7}\left(B^{L}_{\mathrm{m},t,s}\times\alpha_{\mathrm{m},t}\right)\times\sum_{n=1}^{7}\left(B^{W}_{n,t,s}\times\beta_{n,t}\right)\right)\right)} \tag{25}$$

The scenario-based model is chosen to represent uncertainty of wind power in problems. Scenario reduction is performed on the modified system model. The probability of situations is denoted by π_s, $\alpha_{m,t}$, and $\beta_{n,t}$ are the demand probability of electricity consumption and the output probability of wind power at time m and time n, respectively.

Although a large number of scenarios can accurately simulate power load demand and wind energy uncertainty, the computation time and memory required will increase significantly. In this chapter, the fast-marching algorithm is used to reduce the number of generated scenes and accelerate the computational efficiency of the project. Consider the original scene set with N_s scenes and the selected scene set Ψ, and the final selected scene set Ψ_s^* and N_s^* scenes. The steps of the algorithm are as follows:

Step 1: Calculate the distance between each pair of scenes.

Step 2: Calculate the average distance between each scene and other scenes. Select the smallest distance scene as the first selected scene.

Step 3: Calculate the distance between each unselected scene and the selected scene. The scene that minimizes the distance is the next selected scene. The selected and unselected scene sets will be updated.

Step 4: Add the probability of each unselected scene to its nearest selected scene.

In order to solve the SDED problem, 1000 scenes were generated and reduced to 10 scenes by using the fast-marching algorithm.

4.3.2. Objective Function

The overall system consists of four pure power units, two cogeneration units, one pure heat unit, and two units of 55-MW wind turbine. Consider the valve point effect to show the ability of the proposed method. Forecasts of electricity and heat demand take random values between150 MWth and 600 MWth, respectively. Table 5 provides the cost function coefficients of pure power devices. Table 6 lists the cost coefficient of cogeneration units, and Table 7 lists the cost coefficient of only heating units. In addition, Figures 5 and 6 depict the feasible operation area of thermal power of cogeneration units. The parameters related to the wind turbine are shown in Table 8.

Table 5. Cost coefficients for power-only units.

Unit	α	β	γ	λ	ρ	$P^{p,\min}$	$P^{p,\max}$
1	0.008	2	25	100	0.042	10	75
2	0.003	1.8	60	140	0.04	20	125
3	0.0012	2.1	100	160	0.038	30	175
4	0.001	2	120	180	0.037	40	250

Table 6. Cost coefficients for CHP units.

Unit	a	b	c	d	e	f
5	0.0345	14.5	2650	0.03	4.2	0.031
6	0.0435	36	1250	0.027	0.6	0.011

Table 7. Cost coefficients for heat-only unit.

Unit	a	b	c	$H^{\min}$	$H^{\max}$
7	0.038	2.0109	950	0	2695.2

Table 8. Wind turbines parameters.

Rated Power (MW)	Cut-in Speed (m/s)	Rated Speed (m/s)	Cut-Off Speed (m/s)
2	3	13	25

The engineering problem's objective function is defined as follows:

$$OF = \sum_{s=1}^{N_s} \pi_s \sum_{t=1}^{24} \left(\sum_{m=1}^{N_p} C_m(P^p_{m,t,s}) + \sum_{n=1}^{N_c} \left(P^c_{n,t,s}, H^c_{n,t,s}\right) + \sum_{k=1}^{N_h} C_k(H^h_{k,t,s}) \right) \tag{26}$$

where the generation cost of the mth pure power unit in the production of P^p_m MW power is expressed as $C_m(P^p_m)$. $C_n(P^c_n, H^c_n)$ represents the cost of generating P^c_n MW power and H^c_n MWth thermoelectric power from the nth cogeneration unit. $C_k(P^h_k)$ is the power generation cost of pure heat units in the production of H^h_k MWth thermal power. N_p, N_c, and N_h are the entire amounts of pure power, CHP, and pure heat units; m, n, and k are the indicators of the above units. N_s is the total number of scenes, s is the number of scenes index. The cost function and correlation coefficient of the above units are as follows:

$$C_m(P^p_{m,t,s}) = \alpha_m (P^p_{m,t,s})^2 + \beta_m p^p_{m,t,s} + \gamma_m + \left| \lambda_m \sin(\rho_m (P^{p,\min}_m - P^p_{m,t,s}) \right| \tag{27}$$

$$C_n\left(P^c_{n,t,s}, H^c_{n,t,s}\right) = a_n (P^c_{n,t,s})^2 + b_n P^c_{n,t,s} + c_n + d_n (H^c_{n,t,s})^2 + e_n H^c_{n,t,s} + f_n P^c_{n,t,s} H^c_{n,t,s} \tag{28}$$

$$C_k(H^c_{k,t,s}) = a_k (H^h_{k,t,s})^2 + b_k H^h_{k,t,s} + c_k \tag{29}$$

α_m, β_m, γ_m, and ρ_m are the cost coefficients of pure power units; a_n, b_n, c_n, d_n, e_n, and f_n are the cost coefficients of CHP units; a_k, b_k, and c_k are the cost function coefficients related to pure heat units. The current wind speed and wind turbine characteristics constitute the power generation of the wind turbine, the formula is as follows:

$$P_{w,t}^{f} = \begin{cases} 0 & V^t \succ V_{CO}, V^t \prec V_{CL} \\ P^{\max} \times \left(\frac{V^t - V_{CL}}{V_R - V_{CL}}\right) & V_{CL} \le V^t \le V_R \\ P^{\max} & V_R \le V^t \le V_{CO} \end{cases} \tag{30}$$

where $P_{w,t}^{f}$ denotes the wind turbine's expected output at time t. V_{CO}, V_{CL}, and V_R are wind turbine cut-off speed, cut-in speed, and rated speed. When it comes to wind turbines, $P^{\max}$ is the turbine's maximum output power, and V^t denotes the wind speed forecast for time t.

The only equality constraint is the electric heating demand balance equation:

$$\sum_{m=1}^{N_p} P_{m,t,s}^{p} + \sum_{n=1}^{N_h} P_{n,t,s}^{c} = P_{d,t,s} \tag{31}$$

$$\sum_{n=1}^{N_c} P_{m,t,s}^{p} + \sum_{k=1}^{N_h} H_{k,t,s}^{h} = H_{d,t} \tag{32}$$

In the selected Scenario s, the power and thermal energy requirements are $P_{d,t,s}$ and $H_{d,t}$ at time t, respectively. Each unit's yield must fall within the following range:

$$P_m^{p,\min} \le P_{m,t,s}^{c} \le P_m^{p,\max} \tag{33}$$

$$P_n^{c,\min}(H_n^c) \le P_{n,t,s}^{c} \le P_n^{c,\max}(H_n^c) \tag{34}$$

$$H_n^{c,\min}(P_n^c) \le H_{n,t,s}^{c} \le H_n^{c,\max}(P_n^c) \tag{35}$$

$$H_k^{h,\min} \le H_{k,t,s}^{h} \le H_k^{h,\max} \tag{36}$$

where $P_m^{p,\min}$ and $P_m^{p,\max}$ denote the pure power unit's lowest and maximum output powers. $P_n^{c,\min}$ and $P_n^{c,\max}$ denote the lowest and maximum output limitations of a combined heat and power unit, respectively. $H_n^{c,\min}$ and $H_n^{c,\max}$ are the heat output limitations of the CHP unit. $H_k^{h,\min}$ and $H_k^{h,\max}$ represent the top and lower bounds of pure heat units, respectively.

5. Results and Discussion

5.1. Comparative Analysis of CEC2017 Test Function Results

In this paper, the IUVMFO algorithm, MFO algorithm, and DMMFO algorithm in three dimensions of all CEC2017 functions are compared. Due to the limited space, this paper only shows and discusses the algorithm comparison of CEC2017 composite function in 50 dimensions, other comparison results were listed in Tables A3–A5.

The comparative results for the composite text functions in Table 9, Figures 9 and 10 are shown. The suggested IUVMFO outperforms MFO and DMMFO on F29 and F30. It continues to provide apparent benefits in the following seven test functions. DMMFO performs very well on F23 in each dimension and on F24, F25, F27, and F28 in the intermediate and upper dimensions. These five methods, however, are incapable of finding the global optimum solution. Functional tests in 50-dimensional F26 indicate that the two upgraded methods perform worse than the MFO algorithm, while the improved IUVMFO algorithm increases the solution accuracy. As a result, this method performs better than both MFO and DMMFO in the combined test function. The findings above demonstrate that the diversity weight and approach for varying the moth flight route provided in this study greatly increase the algorithm's optimization performance.

Table 9. Statistics of 50-dimensional Function Test Results.

Function		MFO	DMMFO	IUVMFO
F21	Mean	2.679×10^3	2.676×10^3	2.623×10^3
	Std	49.365	30.603	42.085
	Evaluation	+	=	
F22	Mean	1.056×10^4	1.280×10^4	1.012×10^4
	Std	8.093×10^2	5.640×10^2	5.591×10^2
	Evaluation	+	+	
F23	Mean	3.127×10^3	3.126×10^3	3.030×10^3
	Std	63.224	41.230	44.990
	Evaluation	+	=	
F24	Mean	3.194×10^3	3.273×10^3	3.164×10^3
	Std	26.224	43.179	51.141
	Evaluation	-	=	
F25	Mean	5.505×10^3	5.372×10^3	3.603×10^3
	Std	1.737×10^3	9.315×10^2	3.735×10^2
	Evaluation	+	+	
F26	Mean	8.002×10^3	8.231×10^3	7.256×10^3
	Std	5.023×10^2	5.499×10^2	6.000×10^2
	Evaluation	=	+	
F27	Mean	3.522×10^3	3.726×10^3	3.450×10^3

Table 9. *Cont.*

Function		MFO	DMMFO	IUVMFO
	Std	72.958	78.405	73.721
	Evaluation	=	+	
F28	Mean	7.550×10^3	6.966×10^3	7.056×10^3
	Std	1.121×10^3	1.132×10^3	1.475×10^3
	Evaluation	=	-	
F29	Mean	5.156×10^3	5.313×10^3	4.656×10^3
	Std	5.175×10^2	4.464×10^2	4.259×10^2
	Evaluation	+	+	
F30	Mean	3.085×10^3	3.129×10^3	3.060×10^3
	Std	49.062	31.117	64.18
	Evaluation	+	-	
+/−/=/gm		11/3/6/8		

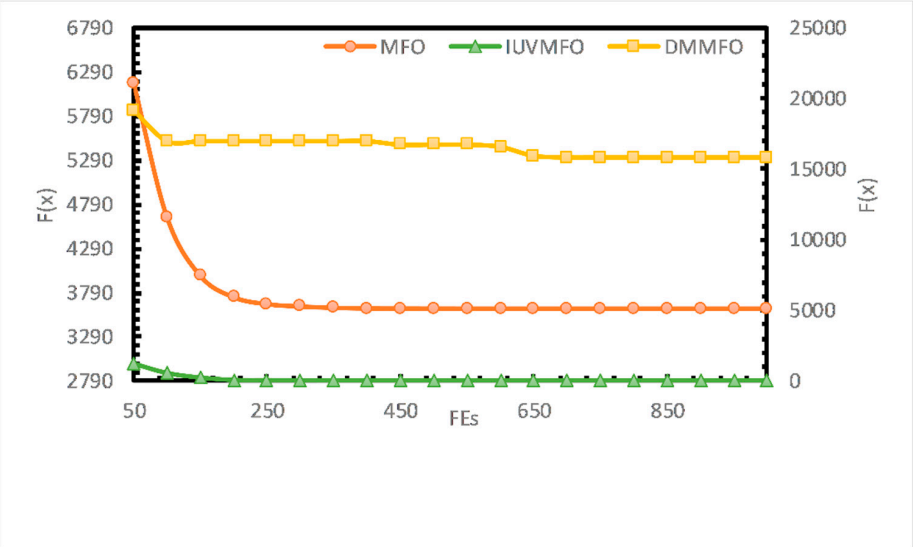

Figure 9. The result curve of F22.

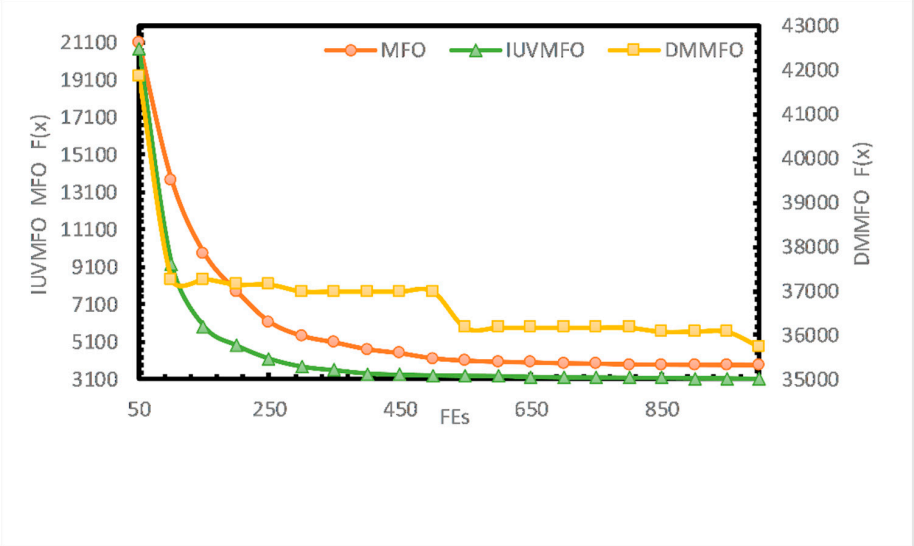

Figure 10. The result curve of F25.

5.2. Comparative Analysis of the Results of Economic Dispatch of Cogeneration

Due to the inevitability of prediction error, the optimal operational process often deviates from the plan (Jiang et al., 2018). In order to further compare the search ability of the algorithm and avoid the randomness of the algorithm, the proposed algorithm and the comparison algorithm are executed 100 times, and the solution changes are shown in Figures 11–13. It should be noted that Table 10 not only reports the best solutions for all solutions but also compares the time spent on 100 runs of various algorithms. In addition, the convergence of their best solutions is shown in Figure 14.

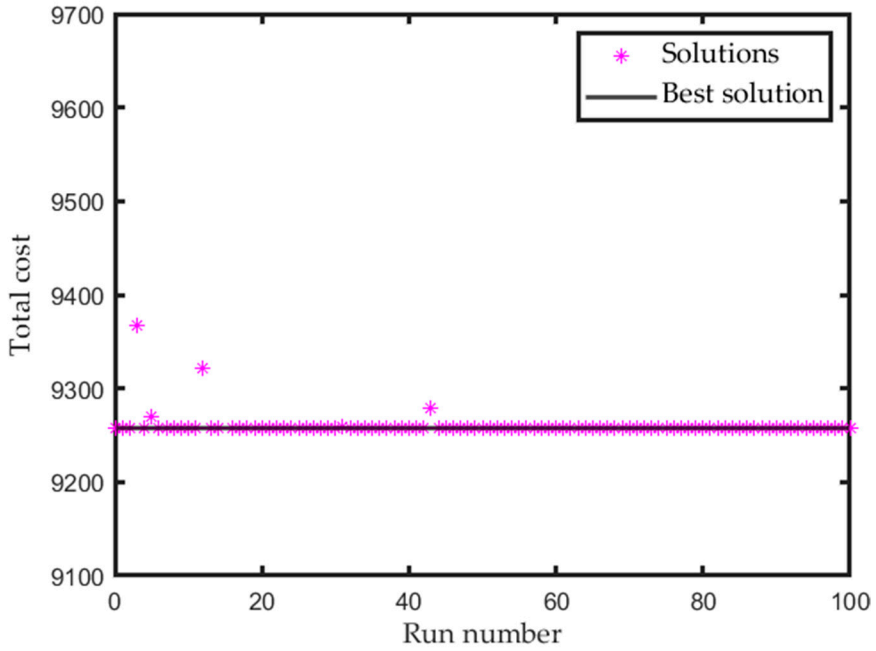

Figure 11. Solution changes for IUVMFO running.

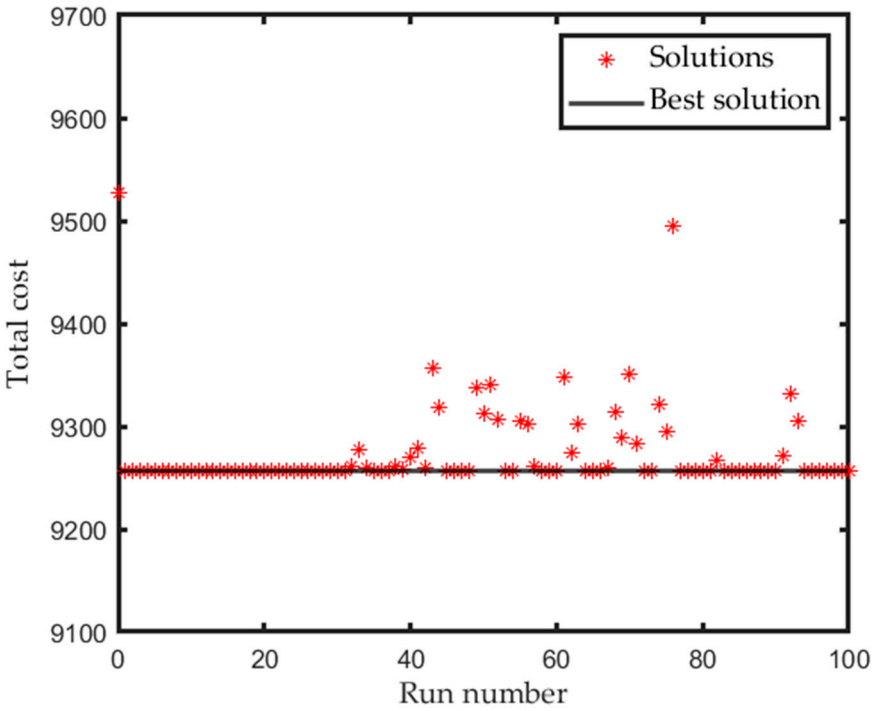

Figure 12. Solution changes for MFO running.

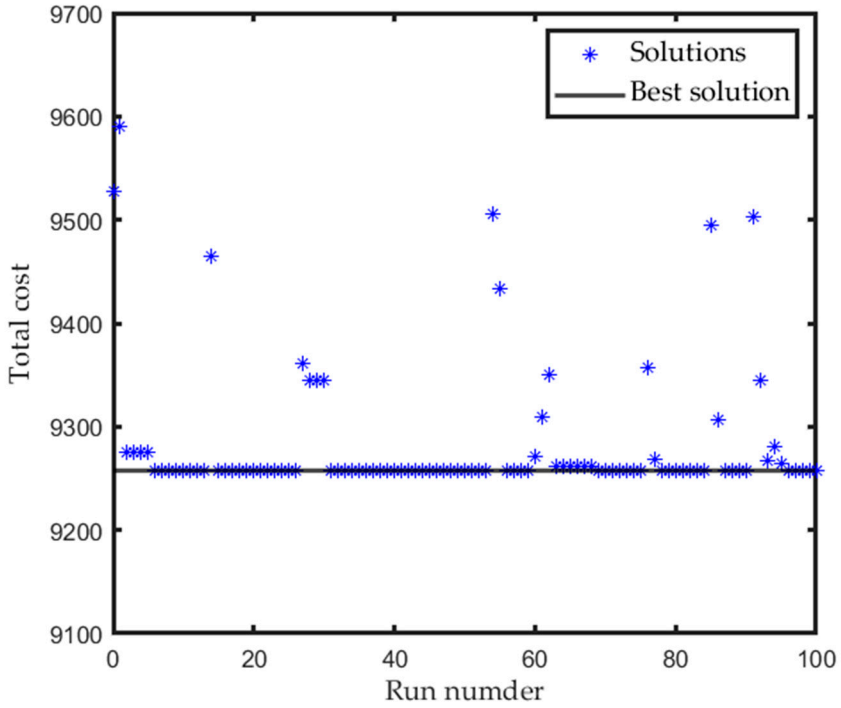

Figure 13. Solution changes for DMMFO running.

Table 10. Comparison of results for economic dispatch of cogeneration.

Algorithm	MFO	DMMFO	IUVMFO
P1 (MW)	0	0	0
P2 (MW)	159	160	160
P3 (MW)	40.097	40	40
H1 (MWth)	91.953	77.740	40
H2 (MWth)	23.738	37.330	75
H3 (MWth)	0	0	0
Cost ($)	9259	9258.7	9257.07
Time (s)	200	100	50

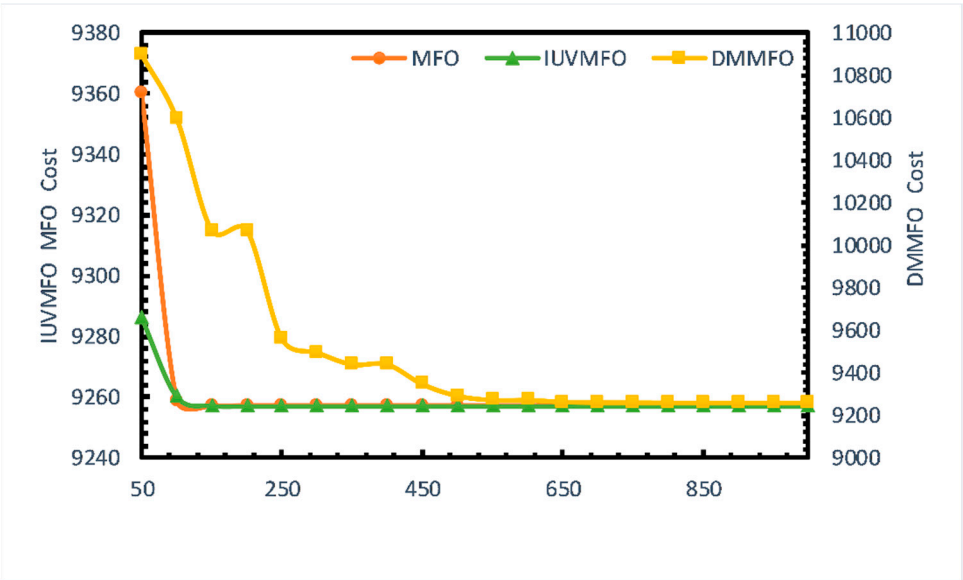

Figure 14. Curve diagram of algorithm test results.

Table 10 shows the cost and running time of different algorithms. The experimental results show that the optimized cost of the IUVMFO algorithm is $9527.075, which is smaller than that of MFO and improved DMMFO and can provide valuable operation strategies. Compared with other algorithms, the IUVMFO algorithm has good optimization performance, strong robustness, and fast convergence speed, which can better solve the problem of economic optimal dispatching of the power system. It can be seen from Figures 11–13 that compared with the MFO algorithm and DMMFO algorithm, the improved IUVMFO algorithm runs 100 times independently in system engineering. It can be seen from the graph that although the convergence results of the objective function of the three algorithms are close, the convergence speed and solution-seeking time are compared. Due to the unified initialization of the IUVMFO algorithm and the improvement of the dynamic variable spiral moth path, the IUVMFO algorithm shows obvious advantages, which can find the best power value faster and smoother, and achieve the goal of minimum cost.

5.3. Comparative Analysis of the Results of Economic Dispatch Considering the Uncertainty of Load and Wind Power

In order to further verify the robustness of the algorithm and solve the constraints of complex power systems and extreme environments, the effectiveness of IUVMFO under three conditions of the integrated energy system was discussed in this section and compared to other algorithms.

5.3.1. Results of Deterministic Dynamic Economic Scheduling Problem

Firstly, the deterministic dynamic economic scheduling problem is solved 100 times, and the results are shown in Table 11. The optimal solution ranges of the IUVMFO algorithm, MFO algorithm, and DMMFO algorithm during 100 runs are shown in Figure 15.

Table 11. Comparison of results for economic dispatch of cogeneration.

Algorithm	MFO	DMMFO	IUVMFO
P1 (MW)	50	54	75
P2 (MW)	30	20	20
P3 (MW)	30	30	30
P4 (MW)	40	95	40
P5 (MW)	81	81	81
P6 (MW)	40	40	40
H1 (MWth)	0	0	0
P7 (MW)	0	0	0
P8 (MW)	128	125	170
Cost ($)	242,231.2	242,231.2	242,231.2
Time (s)	150	130	70

Table 12 shows the cost and running time of different algorithms. The experimental results show that the optimization cost of the IUVMFO algorithm is $242,231.2, which is close to that of the MFO algorithm and the improved DMMFO algorithm. The cost time of IUVMFO decreased 53.3% and 46% compared to the original MFO and DMMFO, respectively. It can be seen from Figure 15 that the IUVMFO algorithm is faster in finding the optimal solution for the cost function. The IUVMFO algorithm has good optimization performance, strong robustness, and fast convergence speed, therefore can better solve the economic optimization scheduling problem of the power system.

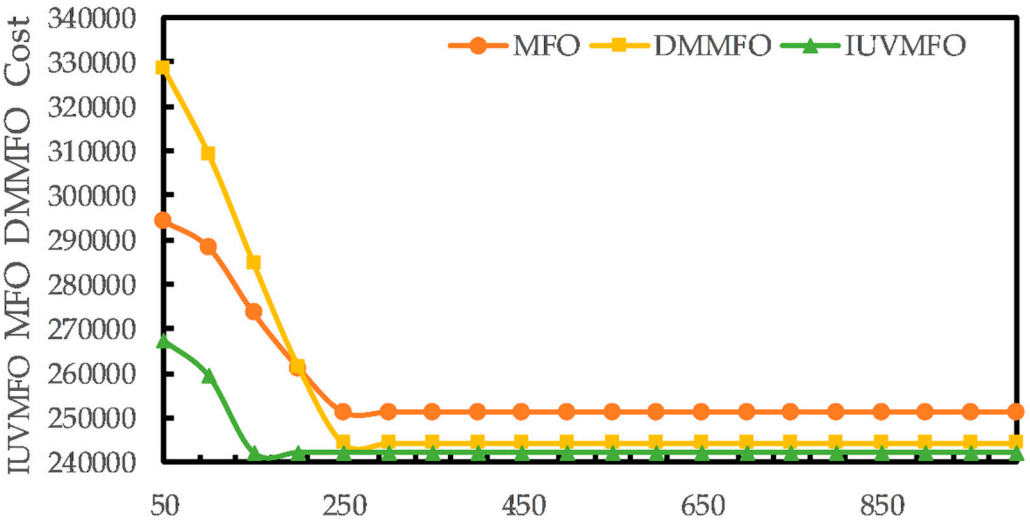

Figure 15. Curve diagram of algorithm test result.

Table 12. Comparison of results for economic dispatch of cogeneration.

Algorithm	MFO	DMMFO	IUVMFO
P1 (MW)	50	54	75
P2 (MW)	30	20	20
P3 (MW)	30	30	30
P4 (MW)	40	95	40
P5 (MW)	81	81	81
P6 (MW)	40	40	40
H1 (MWth)	0	0	0
P7 (MW)	0	0	0
P8 (MW)	128	125	170
Cost ($)	402,171.2	385,762.2	372,457.7
Time (s)	150	130	70

5.3.2. Results of Stochastic Dynamic Economic Scheduling Problem

Due to unavoidable prediction errors in actual operation [32], the uncertainty of power load demand and wind energy are taken into account. Moreover, in order to verify the effectiveness of the proposed method, the uncertainty of power load demand and wind energy are considered in this case.

IUVMFO is carried out in this case compared to MFO and DMMFO. In Table 12, IUVMFO obtained the lowest cost of $372,457.7 and the shortest time of 70 s. The results indicated that the suggested IUVMFO handles this issue successfully and gives the optimal design strategy. However, it can be seen from Figures 16–18 that the stability of the IUVMFO algorithm is better than MFO and DMMFO after 100 independent operation.

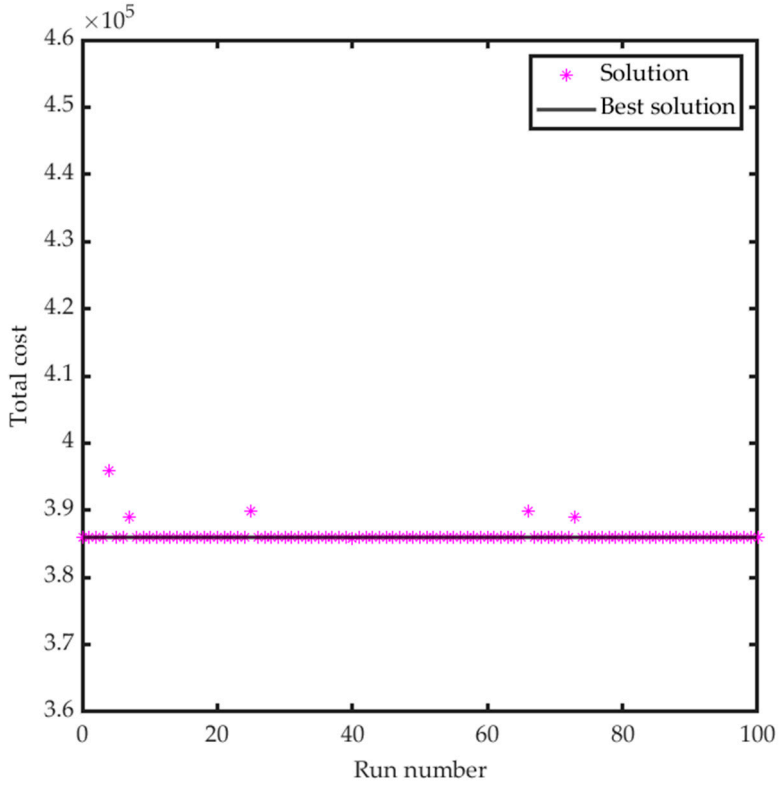

Figure 16. Solution changes for IUVMFO running.

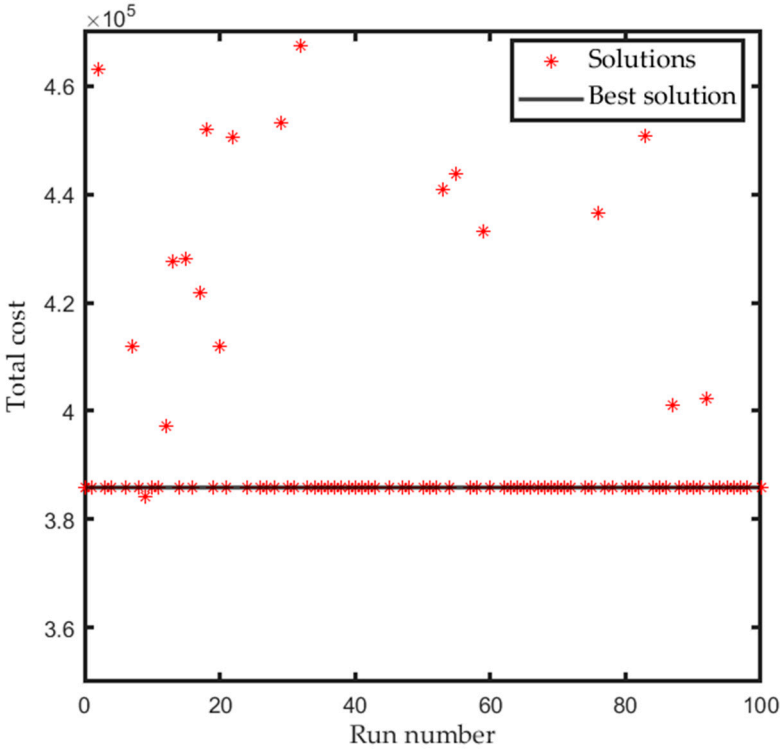

Figure 17. Solution changes for MFO running.

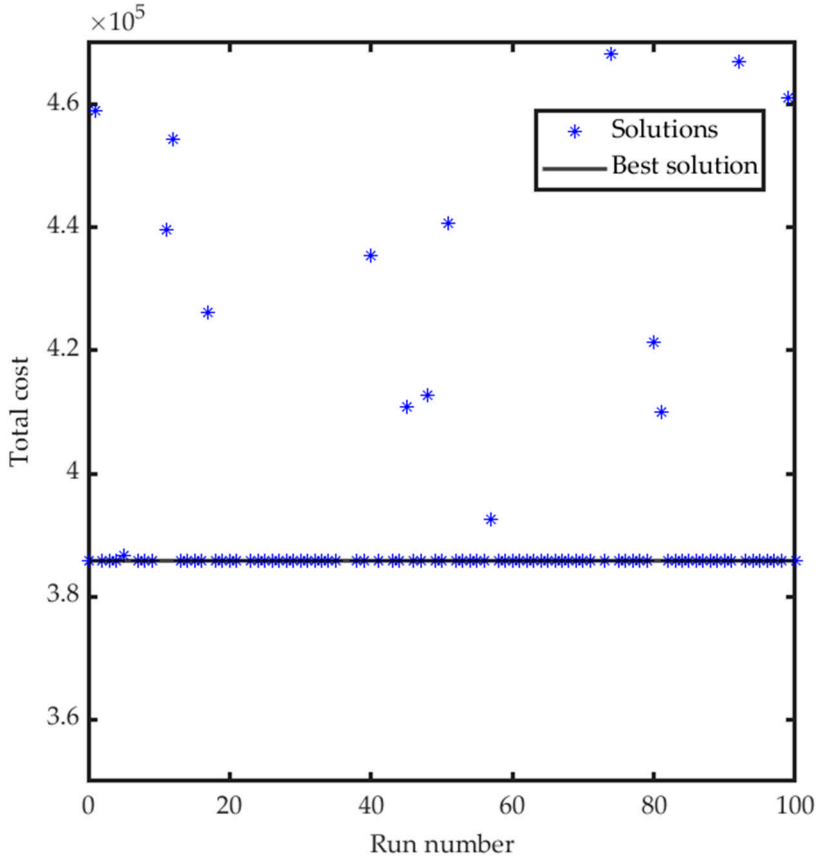

Figure 18. Solution changes for DMMFO running.

It can be seen from Figure 19 that the objective function of the IUVMFO algorithm is the fastest and best to converge to the optimal value in the three algorithms. Whether it is the convergence rate of the solution time, due to the inertia weight of the IUVMFO algorithm and the improvement of the dynamic variable spiral moth path, the IUVMFO algorithm shows obvious advantages. The constraint conditions are used separately to achieve the minimum cost goal and achieve multi-energy complementarity.

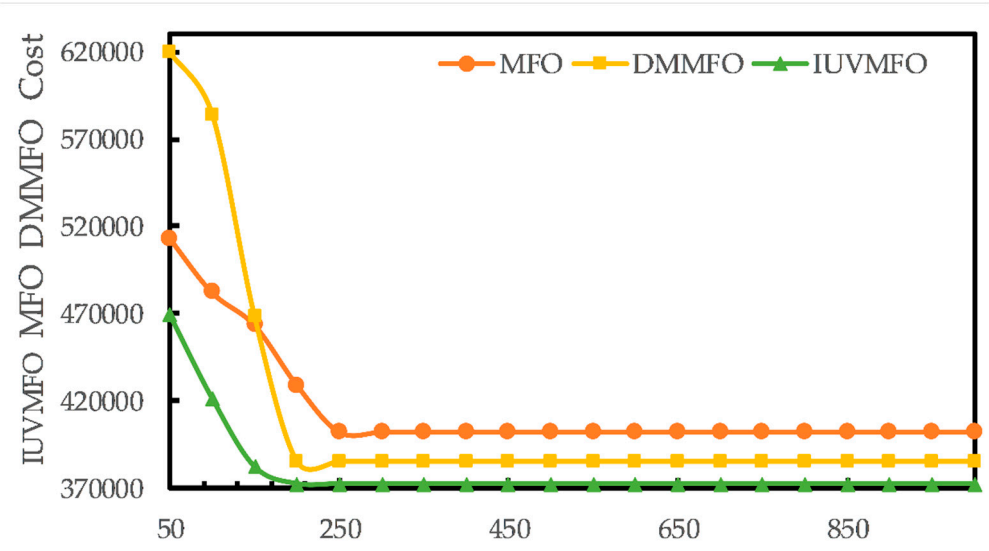

Figure 19. Curve diagram of algorithm test result.

5.3.3. Results of Stochastic Dynamic Economic Scheduling Problem under Extreme Conditions

Three group values of wind speed were tested in this case to verify the effectiveness of IUVMFO under extreme conditions. The detailed wind speed data are given in Table 13.

Table 13. Comparison of results for economic dispatch of cogeneration.

Algorithm	Strong Wind		Weak Wind	
	Cost ($)	Time (s)	Cost ($)	Time (s)
MFO	498,257.2	150	491,257.07	150
DMMFO	485,675.1	130	486,632.2	130
IUVMFO	473,615.2	70	463,214.1	70

We simulate the strong and weak wind environment by amplifying and reducing the 24-h wind speed (Table A6) in the project by a factor of 10, respectively. Through Table 13 and Figures 20 and 21, it can be seen that the operation cost of IUVMFO in two extreme conditions is $473,615.2 and $463,214.1, respectively, which is lower than that of MFO and DMMFO, and the convergence speed of the objective function is better. The proposed method showed satisfactory performance under two extreme conditions and demonstrated better accuracy and speed in convergence.

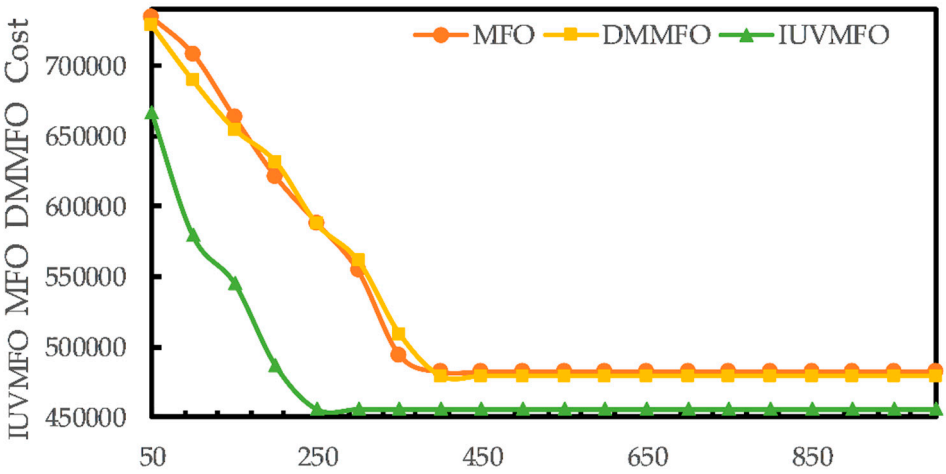

Figure 20. Curve diagram of algorithm test result under strong wind.

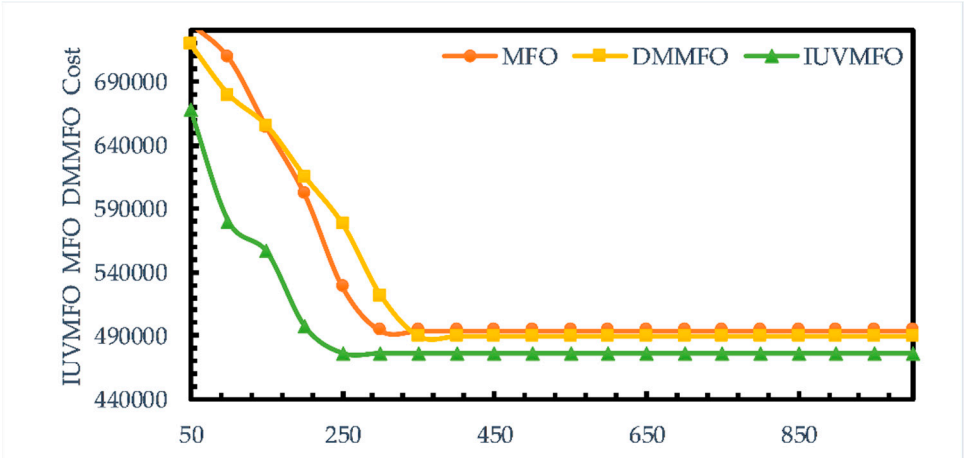

Figure 21. Curve diagram of algorithm test result under weak wind.

6. Conclusions

Three successful enhancement strategies are introduced into MFO in this research to improve the algorithm's performance to overcome premature convergence. First, the moth's solution range is increased by unified initialization. Second, the inertia weight of real-time feedback control is inserted in the particular position update stage. Third, the moth-variable spiral position update approach is implemented. The suggested technique was evaluated using CEC2017 series functions, as well as the average value, standard deviation, and Wilcoxon rank test. The effectiveness of the proposed methods had been verified in the CHP. In the second engineering problem, the deterministic and stochastic problems are introduced, and the system optimization is carried out under extreme conditions. The results show that the IUVMFO algorithm has good optimization performance, strong robustness, and fast convergence speed, which can better solve the economic optimization scheduling problem of the power system. In future work, a multi-objective version of IUVMFO will be developed. In addition, extending IUVMFO to solve discrete optimization tasks is a worthy research direction.

Author Contributions: Conceptualization, F.W. and X.L.; methodology, F.W.; formal analysis, X.L. and N.F.; investigation, Z.J.; resources, X.L. and Z.J.; data curation, N.F.; writing—original draft preparation, F.W.; writing—review and editing, X.L.; funding acquisition, X.L. All authors have read and agreed to the published version of the manuscript.

Funding: This research was supported by the CRSRI Open Research Program (Program SN: CKWV20 18496/KY); National Natural Science Foundation of China, grant number 51809097, 52179016; Open Foundation of Hubei Engineering Research Center for Safety Monitoring of New Energy and Power Grid Equipment, grant number HBSKF202125; Natural Science Foundation of Hubei Province (2021CFB597).

Institutional Review Board Statement: Not applicable.

Informed Consent Statement: Not applicable.

Data Availability Statement: Data is contained within the article.

Conflicts of Interest: The funders had no role in the design of the study; in the collection, analyses.

Appendix A

Table A1. Description of symbols.

Symbol	Description
CHP	the system of combined heat and power
CHPED	the economic dispatch optimization issue of combined heat and power
MFO	moth-flame algorithm
QMFOA	quantum moth flame optimization algorithm
DMMFO	Moth-flame optimization algorithm based on diversity and mutation strategy
CEC2017	Constrained RealParameter Optimization-2017
OF	Objective function
IUVMFO	Improved uniformed variable moth flame optimization algorithm
M	the population of moths
$m_{n,d}$	Single moth position
n	number of moths
d	dimension of optimization problem
OM_n	The fitness of moths
$F_{n,d}$	Single flame position
OF	The fitness of flames
Mi	The ith moth
Fj	The jth flame
S	The spiral function

Table A1. *Cont.*

Symbol	Description
Di	The linear distance between the ith moth and the jth flame
t	A random number between $[-1, 1]$
ω	Inertial weigh
T	Iteration times
$Tmax$	Maximum number of iterations
b	Flight path parameters of moths
k	Flight path adjustment parameters of moths
$X(t)$	Single moth
$X^*(t)$	Flight target location of moths
$MaxFEs$	Iteration times
$C_m(P_m^p)$	the cos t of operation of the mth pure power unit generating P_m^p MW
$C_n(P_n^c, H_n^c)$	the operating cos t of the nth cogeneration unit for the production of P_n^c MW power and H_n^c MWth thermoelectric power
$C_s(H_s^h)$	The operating cos t of the pure heat unit in the production of H_s^h MWth thermal power
N_p	the total number of pure power units
N_c	the total number of CHP units
N_h	the total number of pure heat units
$\alpha_m, \beta_m, \gamma_m$	the calculation coefficients of the operation cost of the mth pure power unit
$a_n, b_n, c_n, d_n, e_n, f_n$	the constant cost coefficients related to the nth CHP unit
a_s, b_s, c_s	the operating cost function coefficients of sth pure heat units
P_d	normal power demand
H_d	normal heat demand
P_{loss}	the transmission loss generated in the whole cogeneration system
$P_m^{p\min}, P_m^{p\max}$	the minimum and maximum electrical power outputs of pure power units
$P_n^{c\min}, P_n^{c\max}$	the minimum and maximum electrical power outputs of CHP unit
$H_n^{c\min}, H_n^{c\max}$	the minimum and maximum electrical power and thermal power outputs of CHP units
$H_s^{h\min}, H_s^{h\max}$	the lower and upper limits of pure thermal units
$C_1(P_1)$	Cost functions for pure power units
$C_4(H_4)$	Cost functions for pure thermal power units
$C_n(P_n^c, H_n^c)$	the cos t of generating P_m^p MW power and H_n^c MWth thermoelectric power from the nth cogeneration unit.
$C_k(P_k^h)$	the power generation cost of pure heat units in the production of MWth thermal power
N_p, N_c, N_h	the entire amount of pure power, CHP, and pure heat units
m,n,k	the indicators of pure power, CHP, and pure heat units
N_s	the total number of scenes
s	the number of scenes index
π_s	The probability of situations
$\alpha_{m,t}, \beta_{n,t}$	the demand probability of electricity consumption and the output probability of wind power at time m and time n
$\alpha_m, \beta_m, \gamma_m, \rho_m$	the cost coefficients of pure power units
$a_n, b_n, c_n, d_n, e_n, f_n$	the cost coefficients of CHP units
a_k, b_k, c_k	the cost function coefficients related to pure heat units
$P_{w,t}^f$	denotes the wind turbine's expected output at time t
V_{CO}, V_{CL}, V_R	wind turbine cut-off speed, cut-in speed, and rated speed
$P^{\max}$	the turbine's maximum
V^t	the wind speed forecast for time t
$P_{d,t,s}, H_{d,t}$	the power and thermal energy requirements of selected scenarios of at time t
$P_m^{p,\min}, P_m^{p,\max}$	the pure power unit's lowest and maximum output powers
$P_n^{c,\min}, P_n^{c,\max}$	the lowest and maximum output limitations of a combined heat and power unit
$H_k^{h,\min}, H_k^{h,\max}$	the top and lower bounds of pure heat units
$\alpha_{i,t}$	The probability of each interval at time t
$B_{(\text{interval},t,s)}^L, B_{(\text{interval},t,s)}^W$	binary parameters of power load demand and time t interval of wind power generation in scene s
$\alpha_{m,t}, \beta_{n,t}$	the demand probability of electricity consumption and the output probability of wind power at time m and time n
σ	Deviation of the prediction error
N_s	original scene
Ψ	the selected scene

Table A2. CEC2017 functions.

No	Functions	Optimum
1	Rotated High Conditioned Elliptic Function	100
2	Rotated Bent Cigar Function	200
3	Rotated Discus Function	300
4	Shifted and Rotated Rosenbrock Function	400
5	Shifted and Rotated Ackley Function	500
6	Shifted and Rotated Weierstrass Function	600
7	Shifted and Rotated Griewank Function	700
8	Shifted Rastrigin Function	800
9	Shifted and Rotated Rastrigin Function	900
10	Shifted Schwefel Function	1000
11	Shifted and Rotated Schwefel Function	1100
12	Shifted and Rotated Katsuura Function	1200
13	Shifted and Rotated HappyCat Function	1300
14	Shifted and Rotated HGBat Function	1400
15	Shifted and Rotated Expanded Griewank plus Rosenbrock Function	1500
16	Shifted and Rotated Expanded Scaffer's F6 Function	1600
17	Hybrid Function1 (N = 3)	1700
18	Hybrid Function2 (N = 3)	1800
19	Hybrid Function3 (N = 4)	1900
20	Hybrid Function4 (N = 4)	2000
21	Hybrid Function5 (N = 3)	2100
22	Hybrid Function6 (N = 5)	2200
23	Composition Function1 (N = 5)	2300
24	Composition Function2 (N = 3)	2400
25	Composition Function3 (N = 3)	2500

Table A2. *Cont.*

No	Functions	Optimum
26	Composition Function4 (N = 5)	2600
27	Composition Function5 (N = 5)	2700
28	Composition Function5 (N = 5)	2800
29	Composition Function5 (N = 5)	2900
30	Composition Function8 (N = 3)	3000
	Search Range: [−100, 100]	

Table A3. Statistics of 50-dimensional Function Test Results.

Function		MFO	DMMFO	IUVMFO
F1	Mean	7.732×10^9	3.324×10^9	2.819×10^9
	Std	5.466×10^9	9.405×10^8	3.336×10^9
	Evaluation	+	=	
F3	Mean	9.166×10^4	1.941×10^5	1.556×10^4
	Std	2.889×10^4	3.735×10^4	1.391×10^4
	Evaluation	+	+	
+/−/=/gm		3/0/1/3		

Table A4. Statistics of 50-dimensional Function Test Results.

Function		MFO	DMMFO	IUVMFO
F4	Mean	3.116×10^3	3.421×10^3	1.424×10^3
	Std	1.557×10^3	1.294×10^3	8.938×10^2
	Evaluation	+	+	
F5	Mean	9.148×10^2	9.703×10^2	8.428×10^2
	Std	73.761	1.224×10^2	53.046
	Evaluation	+	+	
F6	Mean	6.514×10^2	6.499×10^2	6.271×10^2
	Std	8.112	19.116	6.783
	Evaluation	+	+	
F7	Mean	1.766×10^3	1.839×10^3	1.324×10^3
	Std	3.033×10^2	1.584×10^2	1.706×10^2
	Evaluation	+	=	
F8	Mean	1.195×10^3	1.201×10^3	1.150×10^3
	Std	81.074	40.579	32.558
	Evaluation	+	+	
F9	Mean	1.530×10^4	2.468×10^4	8.827×10^3
	Std	4.609×10^4	9.227×10^3	4.629×10^3
	Evaluation	=	+	
F10	Mean	8.298×10^3	1.015×10^4	7.483×10^3
	Std	9.230×10^2	7.322×10^2	7.681×10^2
	Evaluation	+	=	
+/−/=/gm		11/0/3/8		

Table A5. Statistics of 50-dimensional Function Test Results.

Function		MFO	DMMFO	IUVMFO
F11	Mean	1.026×10^4	1.886×10^4	5.284×10^3
	Std	8.015×10^3	1.067×10^4	2.733×10^3
	Evaluation	+	+	
F12	Mean	1.537×10^9	1.791×10^9	9.317×10^8
	Std	1.794×10^9	9.792×10^8	1.273×10^9
	Evaluation	+	=	
F13	Mean	8.406×10^8	2.393×10^8	1.235×10^6
	Std	9.393×10^8	2.671×10^8	5.943×10^6
	Evaluation	+	+	
F14	Mean	1.104×10^6	1.656×10^6	1.973×10^6
	Std	1.604×10^6	2.652×10^6	2.001×10^6
	Evaluation	-	+	
F15	Mean	8.612×10^6	9.225×10^6	3.208×10^4
	Std	2.360×10^7	4.865×10^6	1.252×10^4
	Evaluation	+	+	
F16	Mean	4.249×10^3	3.977×10^3	3.927×10^3
	Std	6.321×10^2	4.689×10^2	4.998×10^2
	Evaluation	+	=	
F17	Mean	3.723×10^3	3.412×10^3	3.485×10^3
	Std	3.006×10^2	2.733×10^2	3.743×10^2
	Evaluation	=	-	
F18	Mean	4.844×10^6	1.524×10^7	2.061×10^6

Table A5. *Cont.*

Function		MFO	DMMFO	IUVMFO
	Std	5.648×10^6	1.724×10^7	4.126×10^6
	Evaluation	+	+	
F19	Mean	1.967×10^6	4.158×10^6	4.259×10^4
	Std	3.742×10^6	2.575×10^6	5.292×10^4
	Evaluation	+	+	
F20	Mean	3.666×10^3	3.560×10^3	3.118×10^3
	Std	4.762×10^2	4.341×10^2	4.182×10^2
	Evaluation	+	+	
+/−/=/gm		15/2/3/13		

Table A6. Wind speed in 24 h.

Time (h)	Wind Speed (m/s)	Time (h)	Wind Speed (m/s)	Time (h)	Wind Speed (m/s)	Time (h)	Wind Speed (m/s)
1	7.95	7	7.15	13	5.1	19	9
2	8.8	8	6.4	14	6.2	20	8.5
3	9.65	9	6.45	15	7.2	21	7.4
4	10.55	10	5.1	16	8	22	7
5	9.45	11	4.35	17	9.35	23	6.75
6	8.45	12	4.7	18	10	24	7.15

References

1. Niknam, T.; Azizipanah-Abarghooee, R.; Roosta, A.; Amiri, B. A new multi-objective reserve constrained combined heat and power dynamic economic emission dispatch. *Energy* **2012**, *42*, 530–545. [CrossRef]
2. Motevasel, M.; Seifi, A.R.; Niknam, T. Multi-objective energy management of CHP (combined heat and power)-based micro-grid. *Energy* **2013**, *51*, 123–136. [CrossRef]
3. Mast, J.; Radle, S.; Gerlach, J.; Bringmann, O. A computational intelligence based approach for optimized operation scheduling of energy plants. *At-Automatisierungstechnik* **2020**, *68*, 118–129. [CrossRef]
4. Li, H.; Jin, Z.L.; Yang, Y.; Huo, Y.W.; Yan, X.; Zhao, P.; Dai, Y.P. Preliminary conceptual design and performance assessment of combined heat and power systems based on the supercritical carbon dioxide power plant. *Energy Convers. Manag.* **2019**, *199*, 111939. [CrossRef]
5. Anh, H.P.H.; Kien, C.V. Optimal energy management of microgrid using advanced multi-objective particle swarm optimization. *Eng. Comput.* **2020**, *37*, 2085–2110. [CrossRef]
6. Zhou, S.Y.; Hu, Z.J.; Gu, W.; Jiang, M.; Chen, M.; Hong, Q.T.; Booth, C. Combined heat and power system intelligent economic dispatch: A deep reinforcement learning approach. *Int. J. Electr. Power* **2020**, *120*, 106016. [CrossRef]
7. Wang, Y.L.; Huang, Y.J.; Wang, Y.D.; Zeng, M.; Li, F.; Wang, Y.L.; Zhang, Y.Y. Energy management of smart micro-grid with response loads and distributed generation considering demand response. *J. Clean. Prod.* **2018**, *197*, 1069–1083. [CrossRef]
8. Li, Z.G.; Wu, W.C.; Shahidehpour, M.; Wang, J.H.; Zhang, B.M. Combined Heat and Power Dispatch Considering Pipeline Energy Storage of District Heating Network. *IEEE Trans. Sustain. Energy* **2016**, *7*, 12–22. [CrossRef]
9. Luo, Y.H.; Yin, Z.X.; Yang, D.S.; Zhou, B.W. A New Wind Power Accommodation Strategy for Combined Heat and Power System Based on Bi-Directional Conversion. *Energies* **2019**, *12*, 2458. [CrossRef]
10. Liu, B.; Li, J.; Zhang, S.; Gao, M.L.; Ma, H.T.; Li, G.Q.; Gu, C.H. Economic Dispatch of Combined Heat and Power Energy Systems Using Electric Boiler to Accommodate Wind Power. *IEEE Access* **2020**, *8*, 41288–41297. [CrossRef]
11. Chen, X.Y.; Kang, C.Q.; O'Malley, M.; Xia, Q.; Bai, J.H.; Liu, C.; Sun, R.F.; Wang, W.Z.; Li, H. Increasing the Flexibility of Combined Heat and Power for Wind Power Integration in China: Modeling and Implications. *IEEE Trans. Power Syst.* **2015**, *30*, 1848–1857. [CrossRef]
12. Mirjalili, S. Moth-flame optimization algorithm: A novel nature-inspired heuristic paradigm. *Knowl.-Based Syst.* **2015**, *89*, 228–249. [CrossRef]
13. Shehab, M.; Alshawabkah, H.; Abualigah, L.; AL-Madi, N. Enhanced a hybrid moth-flame optimization algorithm using new selection schemes. *Eng. Comput.* **2021**, *37*, 2931–2956. [CrossRef]
14. Abd Elaziz, M.; Ewees, A.A.; Ibrahim, R.A.; Lu, S.F. Opposition-based moth-flame optimization improved by differential evolution for feature selection. *Math. Comput. Simul.* **2020**, *168*, 48–75. [CrossRef]
15. Wu, Z.Q.; Shen, D.D.; Shang, M.Y.; Qi, S.Q. Parameter Identification of Single-Phase Inverter Based on Improved Moth Flame Optimization Algorithm. *Electr. Power Compon. Syst.* **2019**, *47*, 456–469. [CrossRef]

16. Pelusi, D.; Mascella, R.; Tallini, L.; Nayak, J.; Naik, B.; Deng, Y. An Improved Moth-Flame Optimization algorithm with hybrid search phase. *Knowl.-Based Syst.* **2020**, *191*, 105277. [CrossRef]
17. Nguyen, T.T.; Wang, H.J.; Dao, T.K.; Pan, J.S.; Ngo, T.G.; Yu, J. A Scheme of Color Image Multithreshold Segmentation Based on Improved Moth-Flame Algorithm. *IEEE Access* **2020**, *8*, 174142–174159. [CrossRef]
18. Taher, M.A.; Kamel, S.; Jurado, F.; Ebeed, M. An improved moth-flame optimization algorithm for solving optimal power flow problem. *Int. Trans. Electr. Energy Syst.* **2019**, *29*, e2743. [CrossRef]
19. Dabba, A.; Tari, A.; Meftali, S. Hybridization of Moth flame optimization algorithm and quantum computing for gene selection in microarray data. *J. Ambient Intell. Humaniz. Comput.* **2021**, *12*, 2731–2750. [CrossRef]
20. Li, Y.; Zhu, X.Y.; Liu, J.S. An Improved Moth-Flame Optimization Algorithm for Engineering Problems. *Symmetry* **2020**, *12*, 1234. [CrossRef]
21. Kaur, K.; Singh, U.; Salgotra, R. An enhanced moth flame optimization. *Neural Comput. Appl.* **2020**, *32*, 2315–2349. [CrossRef]
22. Pradhan, R.; Majhi, S.K.; Jaypuria, J. An orthogonal moth flame optimization for global optimization and application to model order reduction problem. *J. Intell. Fuzzy Syst.* **2020**, *38*, 6649–6661. [CrossRef]
23. Sheng, H.W.; Li, C.Q.; Wang, H.M.; Yan, Z.Y.; Xiong, Y.; Cao, Z.T.; Kuang, Q.Y. Parameters Extraction of Photovoltaic Models Using an Improved Moth-Flame Optimization. *Energies* **2019**, *12*, 3527. [CrossRef]
24. Xu, Y.T.; Chen, H.L.; Heidari, A.A.; Luo, J.; Zhang, Q.; Zhao, X.H.; Li, C.Y. An efficient chaotic mutative moth-flame-inspired optimizer for global optimization tasks. *Expert Syst. Appl.* **2019**, *129*, 135–155. [CrossRef]
25. Yu, C.Y.; Heidari, A.A.; Chen, H.L. A quantum-behaved simulated annealing algorithm-based moth-flame optimization method. *Appl. Math. Model.* **2020**, *87*, 1–19. [CrossRef]
26. Zhang, J.; Sheng, J.N.; Lu, J.W.; Shen, L. UCPSO: A Uniform Initialized Particle Swarm Optimization Algorithm with Cosine Inertia Weight. *Comput. Intell. Neurosci.* **2021**, *2021*, 8819333. [CrossRef]
27. Jiang, Z.Q.; Song, P.B.; Liao, X. Optimization of Year-End Water Level of Multi-Year Regulating Reservoir in Cascade Hydropower System Considering the Inflow Frequency Difference. *Energies* **2020**, *13*, 5345. [CrossRef]
28. Liu, L.; Bai, K.; Dan, Z.; Zhang, S.; Liu, Z. Whale Optimization Algorithm with Global Search Strategy. *J. Chin. Comput. Syst.* **2020**, *41*, 1820–1825.
29. Ma, L.; Wang, C.; Xie, N.G.; Shi, M.; Ye, Y.; Wang, L. Moth-flame optimization algorithm based on diversity and mutation strategy. *Appl. Intell.* **2021**, *51*, 5836–5872. [CrossRef]
30. Sohrabi, F.; Jabari, F.; Pourghasem, P.; Mohammadi-Ivatloo, B. Combined Heat and Power Economic Dispatch Using Particle Swarm Optimization. In *Optimization of Power System Problems: Methods, Algorithms and MATLAB Codes*; Pesaran Hajiabbas, M., Mohammadi-Ivatloo, B., Eds.; Springer International Publishing: Cham, Switzerland, 2020; pp. 127–141.
31. Pourghasem, P.; Sohrabi, F.; Jabari, F.; Mohammadi-Ivatloo, B.; Asadi, S. Combined Heat and Power Stochastic Dynamic Economic Dispatch Using Particle Swarm Optimization Considering Load and Wind Power Uncertainties. In *Optimization of Power System Problems: Methods, Algorithms and MATLAB Codes*; Pesaran Hajiabbas, M., Mohammadi-Ivatloo, B., Eds.; Springer International Publishing: Cham, Switzerland, 2020; pp. 143–169.
32. Jiang, Z.Q.; Li, R.B.; Li, A.Q.; Ji, C.M. Runoff forecast uncertainty considered load adjustment model of cascade hydropower stations and its application. *Energy* **2018**, *158*, 693–708. [CrossRef]